Electrical Power and Energy Systems 171 (2025) 111020

Contents lists available at ScienceDirect

International Journal of Electrical Power and Energy Systems

journal homepage: www.elsevier.com/locate/ijepes

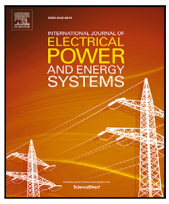

The impact of electricity network and generator models on the accuracy and computational efficiency of multi-energy system investment and operation planning

Zhi Gao [a], Germán Morales-España [b,c], Madeleine Gibescu [a], Matteo Gazzani [a,d,*]

[a] Copernicus Institute of Sustainable Development, Utrecht University, Utrecht, 3584CS, The Netherlands
[b] TNO Energy Transition, The Netherlands
[c] Faculty of Electrical Engineering, Mathematics and Computer Science, Delft University of Technology, The Netherlands
[d] Sustainable Process Engineering Chemical Engineering and Chemistry, Eindhoven University of Technology, Eindhoven, 5612 AP, The Netherlands

ARTICLE INFO

Keywords:
Energy system optimization
Power flow equations
Transmission losses
Unit commitment

ABSTRACT

As energy sectors become increasingly interconnected, selecting appropriate representations of physical characteristics in energy system optimization models has become challenging. This study evaluates the necessity of transmission and generator models by systematically excluding each one and assessing the impact on objective values, solution time, and feasibility of the resulting system design. We apply this analysis to two contrasting case studies optimizing the design and operation of: the IEEE 118-bus test power system and a zero-emission multi-energy system of the Netherlands. Results show that modeling Kirchhoff's Voltage Law (KVL) and alternating-current (AC) transmission losses is essential for accuracy and feasibility. KVL prevents unrealistic network loops; hence improving network utilization. Additionally, we evaluate two linearization methods for the AC transmission losses. Our findings indicate that tangent-based linear approximations often lead to infeasibility with three or fewer segments, whereas a piecewise-linear approach with at least two segments ensures accurate and computationally efficient solutions.

1. Introduction

To meet climate goals, major economies in the world are taking steps to transform their energy systems to reduce the emission of greenhouse gases [1,2]. In this rapid transition towards sustainable energy systems, Energy System Optimization Models (ESOMs) have gained widespread use as a tool for policy-making and decision support.

An ESOM consists of a set of parameters, equality and inequality constraints that represent the physical nature of an energy system. By adding an objective function that reflects the goals of the decision maker (such as minimizing costs and/or greenhouse gas emissions for optimal system investment and/or operation planning) and the associated decision variables, the ESOM is cast as a mathematical optimization problem. As in all models, the solution quality depends on the level of detail of the representation. However, higher accuracy often means higher computational costs, which may make a problem unfeasible [3]. At the same time, with the ongoing integration of renewable energy sources, the emergence of hydrogen technologies and the interdependence between energy sectors, building more comprehensive ESOMs has become imperative for obtaining reliable and relevant outcomes. Consequently, ESOM developers face the challenge of selecting a representation that balances accuracy with computational tractability for planning and operation decisions in future energy systems [4,5].

When it comes to ESOM representation, studies focused on power system planning and operation are distinct from other, cross-sectoral energy system models: The former put most modeling efforts on the power generation and on the electricity grid, as seen in [6–8]. Other energy carriers, if considered, are usually treated as a source of electricity generation or demand [9,10]. With such focus, ESOM studies in the power system domain typically have more intricate descriptions of the physical phenomena, mainly in electricity transmission and the flexibility of generators. In terms of electricity transmission, power-flow equations are often modeled in the simplified linear version (DC power flow), which is necessary to retain linear programming. While various ways of modeling the transmission losses are commonly adopted [11]. It has been shown that neglecting or oversimplifying these transmission features can lead to infeasible grid planning [12]. Another standard practice is to model the flexibility of thermal electricity generators, including the ramp rate, discrete unit commitment, minimum output level, and minimum up and down time [13]. More recently, researchers also incorporated output trajectories of the unit start-up and shut-down

* Corresponding author at: Copernicus Institute of Sustainable Development, Utrecht University, Utrecht, 3584CS, The Netherlands.
E-mail address: m.gazzani@uu.nl (M. Gazzani).

https://doi.org/10.1016/j.ijepes.2025.111020
Received 29 April 2025; Received in revised form 7 August 2025; Accepted 13 August 2025
Available online 27 August 2025

Nomenclature

Sets

$\mathcal{T}$	Time steps
$\mathcal{N}$	Geographical nodes
$\mathcal{C}$	Energy carriers
$\mathcal{L}$	Energy transport lines
$\mathcal{K}$	Energy conversion (including generation) and storage technologies

Decision variables

f	Energy flow
θ	Phase angle
ψ	Energy loss
d	Discrete unit investment
α	Invested technology capacity
e^{output}	Energy output
$\hat{e}$	Energy output above minimum level
e^{input}	Energy input
u	Clustered unit commitment
y	Start up units
z	Shut down units
γ	Binary status of charging or discharging storage
ϕ	Stored energy

Parameters

R	Electric line resistance
$\tilde{R}$	Electric line resistance per unit distance
X	Electric line reactance
$\tilde{X}$	Electric line reactance per unit distance
$\overline{\alpha}$	Maximum investment limit
E	Unit capacity
$\underline{E}$	Minimum power output
SU	Power output during start-up
SD	Power output during shut-down
TU	Minimum time up
TD	Minimum time down
P^{SU}	Power output on the start-up trajectory
P^{SD}	Power output on the shut-down trajectory
SUD	Start-up duration
SDD	Shut-down duration
RD	Maximum ramp-down rate
RU	Maximum ramp-up rate
C^I	Investment cost
$\tilde{C}^I$	Investment cost per unit distance for transmission lines
C^O	Generation cost
C^{SU}	Start-up cost
L	Distance of line connection
F	Transport line capacity
Y	Design lifetime
β	Loss coefficient of hydrogen pipelines
η	Efficiency
WA	Area for wind turbines
WA^0	Average area per wind turbine
E^{avail}	Available wind power
V	Wind speed
SA	Area for solar PV
I	Solar irradiance
σ	Self-dissipation rate of battery
ϵ	Ratio of compression work to store hydrogen
D	Discrete unit investment limit

Other symbols

P	Active power
Q	Reactive power
V	Voltage magnitude
Ψ	Transmission loss
m	Slope
a	Offset
h	Height
h^0	Reference height
NPV	Net present value
FOM	Fixed operation & maintenance cost factor

period [14]. While incorporating these detailed flexibility characteristics can be computationally demanding, it often ensures the solution quality in power system ESOM studies [15].

Despite their standard use in the power system domain, it remains unclear to what extent power transmission physics and generator flexibility characteristics need to be included in multi-sector ESOM studies. This is a challenge because, when modeling multiple energy carriers in hourly resolution for a chosen design year, even without intricate details, the solutions tend to be computationally expensive. For example, a multi-sector ESOM applied to the French national system in hourly resolution takes more than 60 h to solve [16]. In this case, none of the transmission details and only ramp rate limits are considered for thermal generation units. That being said, simplification methods in the temporal aspects of ESOMs have proven their capability to reduce the computational cost significantly while bringing only small errors to the solution [17,18]. This opens up spaces for having a higher level of detail in the technological aspect. However, to the best of our knowledge, the computational costs and accuracy benefits of including the more realistic power transmission and generator flexibility characteristics in multi-energy ESOMs have not yet been investigated, despite their ubiquity in the power system scientific community.

The necessity of including the power system characteristics faces another layer of uncertainty when emerging energy technologies exhibit greater responsiveness and flexibility. Consider hydrogen technologies as an example. Alkaline [19] and especially Proton Exchange Membrane (PEM) [20] water electrolyzers can reportedly ramp up to their full capacity within a few minutes with even faster ramp-down capabilities [21]. Restarting their operation with a complete system purge takes less than an hour [21,22]. Moreover, PEM fuel cells are able to “cold start”, initiating from subzero ambient temperature within 100 s [23], and can adjust their operational level in a few seconds [24]. For ESOMs that are typically hourly-resolved, these hydrogen technologies are less constrained than the thermal power plants to respond to temporal fluctuations of demand and available renewable power. The balance of energy across different locations can therefore be reinforced by adding a hydrogen network and associated conversion technologies. Both the power output by the thermal power plants and the power flow on the transmission lines may exhibit more stable profiles when hydrogen-related technologies are present. Consequently, the power system characteristics could make little to no difference in the problem solution. The necessity of including power system characteristics under such circumstances has not yet been analyzed

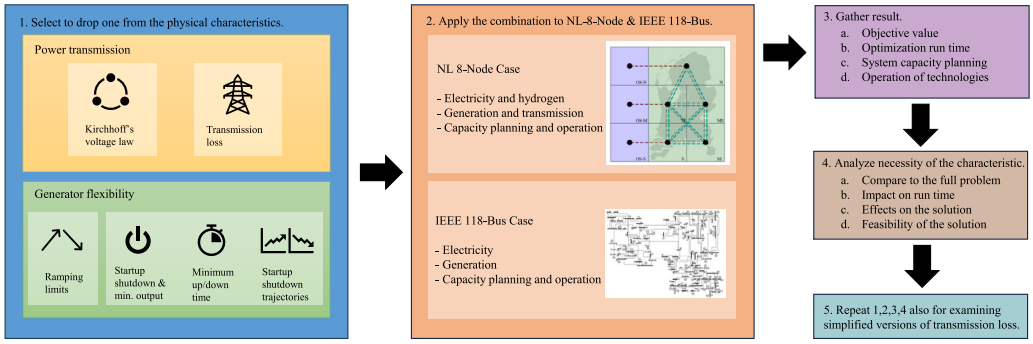

Fig. 1. Methodology of determining the necessity of power system characteristics in this study.

and can be subject to debate. Thus, it becomes crucial to evaluate and compare different modeling approaches in ESOMs. When looking at existing scientific literature, while numerous studies assess techniques in time-series aggregation, such as [25–28], only a few studies offer comparative evaluations of the modeling approaches concerning physical details of the power grid and associated energy conversion technologies.

For example, Helistö et al. [5] analyzed the impacts of both time-series aggregation and operational details on investment planning. They emphasize capturing cross-sectoral interactions when selecting modeling approaches. Nevertheless, the results are based on case studies that neglect the power grid and relevant constraints. Priesmann et al. [29] provides a comprehensive review of model simplification approaches, including the time horizon and resolution, electricity grid transmission loss, spatial resolution, and plant clustering in the network, among other operational details. However, their analysis is primarily focused on power systems and lacks consideration of interactions with other energy sectors. Furthermore, the study considered an approximation of the transmission loss and omitted Kirchhoff's Voltage Law (KVL), which, next to Kirchhoff's Current Law (KCL) and Ohm's law, forms the basis of the AC power-flow principles.

On the other hand, Neumann et al. [12] compared linear approximations to the electricity transmission loss with and without KVL, using an EU-wide power system model. Their findings underscore the indispensable nature of KVL in modeling the electricity network. Interestingly, they demonstrate that linear approximations with as few as three pieces suffice for accurately modeling the quadratic transmission loss. Yet, it is worth noting that their study focuses on optimizing the investment and operation of the power sector with local hydrogen storage. They do not consider the possibility of a hydrogen network alleviating electricity grid congestion and providing additional flexibility.

Other than the network details, Wuijts et al. [3] conducted a comparative study on modeling the generator unit commitment. The study presents linear formulations and simplifications of the unit start-up and shut-down, minimum up- and downtime, ramp rate limits and the cost function, as well as their impacts on the computational cost and solution quality. Using a series of cases, they identify two prospective simplifications, namely a single-piece linear technology cost and the linear relaxation of the commitment variables. Other simplifications are deemed harmful to the solution's accuracy, regardless of their reductions in computational cost. Nevertheless, the study has the lenses also focused on power system cases.

For the planning of future energy systems featuring electricity grids and true integration of multiple energy sectors, we lack evidence-based reasoning in determining which physical details are essential to model in detail and which can be simplified. Inspired by this research gap, we put forward the methodology of this study, as illustrated in Fig. 1. Firstly, we examine the importance of power transmission and generator flexibility characteristics in the operation of the IEEE 118-bus test system, which anchors the work in the classical power system literature. Then we apply different combinations of modeling choices to a multi-energy ESOM that addresses both the planning and operation of a future electricity-hydrogen system for the Netherlands. We evaluate the necessity of modeling each of the characteristics by assessing the resulting system designs and computational costs when we remove the characteristics one by one.

The novel contributions of this work are summarized below:

1. We systematically test the effects of using different modeling approaches for the electricity transmission and technology characteristics in *both* power and multi-energy system applications.
2. We evaluate the effects that the different approaches have on the selection, sizing, and operation of different conversion and storage technologies, and on the electricity and hydrogen grids.
3. We evaluate the effects that the different approaches have on the solution quality, e.g., feasibility of designs obtained from simpler models in the operation of more realistic ones, and on the computational performance.
4. We investigate the role of different modeling choices to linearize the quadratic electricity transmission loss.

The remainder of this paper is structured as follows. Section 2 introduces the model formulations used for power transmission and generator flexibility characteristics. This is followed by elaborating on the implementation of the characteristics and the design of a case study in Section 3. Results and discussion are presented in Section 4. Finally, the paper concludes with recommendations on selecting and modeling the relevant physical characteristics in Section 5.

2. Formulation of physical characteristics in energy system optimization

In the following, we discuss how certain physical characteristics are traditionally included in linear (power) ESOM, more specifically: (i) Kirchhoff's voltage law, (ii) network losses, (iii) dynamic features of generators in unit commitment. Prior to this, we start by presenting a basic formulation of an energy system optimization problem. The full formulation is a mixed-integer linear programming (MILP) model.

2.1. Basic formulation of an energy system optimization problem

2.1.1. Nodal energy balance

The energy balance holds for each node n, energy carrier c and time step t.

$$D_{n,c,t} = \sum_{l \in \mathcal{L}_{n,c}^{\text{inflow}}} (f_{l,t} - \frac{1}{2}\psi_{l,t}) - \sum_{l \in \mathcal{L}_{n,c}^{\text{outflow}}} (f_{l,t} + \frac{1}{2}\psi_{l,t}) + \sum_{k \in \mathcal{K}_{n,c}^{\text{output}}} e_{k,t}^{\text{output}} - \sum_{k \in \mathcal{K}_{n,c}^{\text{input}}} e_{k,t}^{\text{input}} \quad \forall n \in \mathcal{N}, c \in C, t \in \mathcal{T} \tag{1}$$

where $D_{n,c,t}$ is the demand. $\mathcal{L}_{n,c}^{\text{inflow}}$ denotes the set of lines transmitting carrier c with the default direction arriving at node n, and $\mathcal{L}_{n,c}^{\text{outflow}}$ is

the set of lines leaving from node n. f_{lt} is the energy flow on line l with its sign denoting the flow direction. $K_{n,c}^{\text{output}}$ and $K_{n,c}^{\text{input}}$ are the sets of technologies at node n that output and input energy carrier c, respectively. $e_{k,t}^{\text{output}}$ and $e_{k,t}^{\text{input}}$ are the corresponding energy output and input. $\mathcal{N}$ is the set of geographical nodes, C the set of energy carriers, and $\mathcal{T}$ the set of time steps.

2.1.2. Investment decisions

For HVDC lines and hydrogen pipelines that can be continuously invested, the invested capacity α has a maximum value $\overline{\alpha}$ for each line l,

$$0 \le \alpha_l \le \overline{\alpha}_l \qquad \forall l \in \mathcal{L}^{\text{DC}} \cup \mathcal{L}^{\text{H}_2} \tag{2}$$

The energy flow f on these transmission lines is limited by the invested capacity α for every time step t:

$$-\alpha_l \le f_{lt} \le \alpha_l \qquad \forall l \in \mathcal{L}^{\text{DC}} \cup \mathcal{L}^{\text{H}_2}, t \in \mathcal{T} \tag{3}$$

For AC transmission lines that can only be discretely invested in, the energy flow has a range of

$$-F_l d_l \le f_{lt} \le F_l d_l \qquad \forall l \in \mathcal{L}^{\text{AC}}, t \in \mathcal{T} \tag{4}$$

where F_l is the fixed capacity of a transmission line, and $d_l \in \{0,1\}$ the binary investment decision We do not consider the investment of parallel lines, due to the nonlinear effects on the line reactance.

For the thermal generation units that are built discretely, the integer investment decision $d_k \in \mathbb{N}$ in the number of units has a maximum limit. The invested capacity is then the invested units times the unit capacity E_k, which forms the upper bound of the generation output $e_{k,t}^{\text{output}}$.

$$0 \le e_{k,t}^{\text{output}} \le E_k d_k \le E_k \overline{d}_k \quad \forall k \in \mathcal{K}^{\text{thermal}}, t \in \mathcal{T} \tag{5}$$

There are also upper limits for continuous investments in the other conversion (including generation) and storage technologies, which decide their maximum energy output and input, given as

$$0 \le e_{k,t}^{\text{output}} \le \alpha_k \le \overline{\alpha}_k \quad \forall k \in \mathcal{K} \setminus \mathcal{K}^{\text{thermal}}, t \in \mathcal{T} \tag{6}$$

$$0 \le e_{k,t}^{\text{input}} \le \alpha_k \le \overline{\alpha}_k \quad \forall k \in \mathcal{K}^{\text{storage}}, t \in \mathcal{T}. \tag{7}$$

2.1.3. Status of storage technologies

In terms of the energy storage technologies, their status can switch between charging and discharging according to

$$e_{k,t}^{\text{input}} \le \overline{\alpha}_k (1 - \gamma_{k,t}) \qquad \forall k \in \mathcal{K}^{\text{storage}}, t \in \mathcal{T} \tag{8}$$

$$e_{k,t}^{\text{output}} \le \overline{\alpha}_k \gamma_{k,t} \qquad \forall k \in \mathcal{K}^{\text{storage}}, t \in \mathcal{T} \tag{9}$$

where $e_{k,t}^{\text{input}}$ is the energy input, $e_{k,t}^{\text{output}}$ is the energy output, and γ a binary decision variable for the charging/discharging status. The stored energy $\phi_{k,t}$ is dependent on that of the previous time step and the current energy input or output. At the first time step, this inter-temporal energy balance is linked to the end of the horizon, i.e., the last time step.

$$\phi_{k,t} = (1 - \sigma_k)\phi_{k,|T|} + \eta_k e_{k,t}^{\text{input}} - e_{k,t}^{\text{output}} \quad \forall k \in \mathcal{K}^{\text{storage}}, t \in \mathcal{T} | t = 1 \tag{10}$$

$$\phi_{k,t} = (1 - \sigma_k)\phi_{k,t-1} + \eta_k e_{k,t}^{\text{input}} - e_{k,t}^{\text{output}} \quad \forall k \in \mathcal{K}^{\text{storage}}, t \in \mathcal{T} | t > 1 \tag{11}$$

where σ_k is the self-dissipation rate of the battery system. η_k is the cycle efficiency. For each storage technology unit, we assume that the storage volume is proportional to the invested output (and input) capacity.

$$0 \le \phi_{k,t} \le \text{EPR}_k \alpha_k \quad \forall k \in \mathcal{K}^{\text{storage}}, t \in \mathcal{T} \tag{12}$$

where EPR_k is the energy-to-power ratio.

2.2. Electric circuit laws: Kirchhoff's voltage law

Kirchhoff's Voltage Law is often overlooked among the power transmission formulations in multi-energy ESOMs: Commonly adopted is the energy balance (i.e., that the energy imported and converted must be equal to the energy leaving and consumed at a given location, including the losses), which in electric circuit theory translates to Kirchhoff's Current Law (KCL). By combining Ohm's law with KVL, the AC power flow equations give the active and reactive power flow P_{ij} and Q_{ij} from bus i to bus j for all three phases, if we assume symmetric loading, as,

$$P_{ij} = 3\frac{X_{ij}V_iV_j \sin(\theta_i - \theta_j) + R_{ij}[V_i^2 - V_iV_j \cos(\theta_i - \theta_j)]}{R_{ij}^2 + X_{ij}^2} \tag{13}$$

$$Q_{ij} = 3\frac{X_{ij}[V_i^2 - V_iV_j \cos(\theta_i - \theta_j)] - R_{ij}V_iV_j \sin(\theta_i - \theta_j)}{R_{ij}^2 + X_{ij}^2} \tag{14}$$

where V_i, V_j are the single-phase voltage magnitudes at buses i and j, θ_i and θ_j the bus voltage angles. R_{ij} and X_{ij} are the resistance and reactance of the line between buses i and j, respectively.

Linearization is necessary to include this characteristic in large-scale ESOMs with reasonable computational cost. According to the well-known linear approximation of the power flow equations DC-OPF, we can simplify (13)–(14) by assuming that the voltages at the buses have similar magnitudes [30].

$$V_i \approx V_j \approx V \tag{15}$$

The phase angle difference is small; therefore

$$\sin(\theta_i - \theta_j) \approx \theta_i - \theta_j \tag{16}$$

$$\cos(\theta_i - \theta_j) \approx 1 \tag{17}$$

Finally, the reactance is much larger than the resistance,

$$X_{ij} \gg R_{ij} \tag{18}$$

Hence, the active and reactive power in (13) and (14) can be approximated to:

$$P_{ij} \approx 3V^2 \frac{\theta_i - \theta_j}{X_{ij}} = \frac{\theta_i - \theta_j}{X_{ij}^{\text{PU}}} \tag{19}$$

$$Q_{ij} \approx 0 \tag{20}$$

where X_{ij}^{PU} is the per unit (p.u.) reactance between buses i and j and all voltages are assumed equal to 1 p.u. It should be noted that the linearization of the power flow equations states that the active power flow is dependent on the difference between voltage angles and inversely proportional to the line reactance, as shown in (19). Conversely, the reactive power flow is neglected and the voltage profile is assumed flat across all buses in the network.

When we implement KVL in an energy system optimization problem, we use more generic nodes n instead of the buses. And we represent (19) with

$$f_{l,t} = \frac{\theta_{n^i(l)} - \theta_{n^j(l)}}{X_l^{\text{PU}}} \quad \forall l \in \mathcal{L}^{\text{AC}} \tag{21}$$

where $f_{l,t}$ is the flow on line l at time step t. $n^i(l)$ and $n^j(l)$ are the starting and ending nodes of the line, respectively.

2.3. Electric circuit laws: approximations of AC transmission losses

The transmission loss can be derived as the difference between the power sent and received along a network element, such as a power line or transformer.

$$\Psi_{ij} = P_{ij} + P_{ji} \tag{22}$$

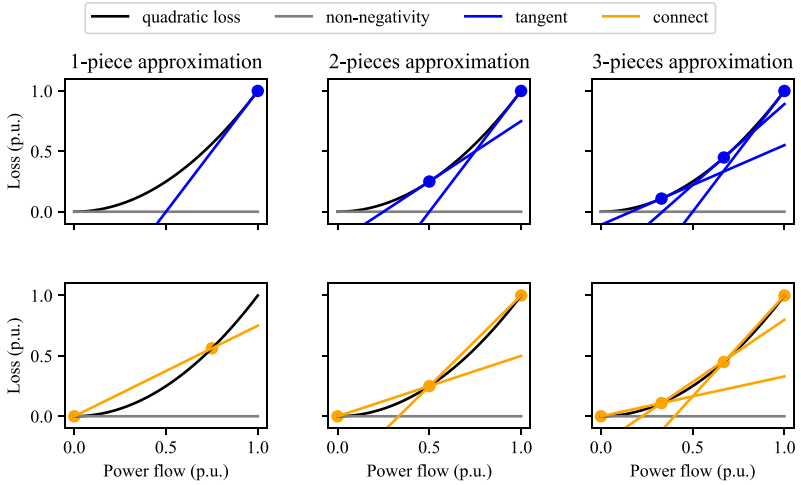

Fig. 2. Linear approximations to the quadratic AC transmission loss, top 3 figures showing the method using tangents, and the bottom 3 showing the method by connecting the points.

Using the terms from (13), we have

$$\Psi_{ij} = \frac{3R_{ij}}{R_{ij}^2 + X_{ij}^2}(V_i^2 + V_j^2 - 2V_iV_j\cos(\theta_i - \theta_j)) \tag{23}$$

Furthermore, we apply the assumption of similar voltage magnitudes as in (15) and the following more accurate version of the phase angle difference:

$$\cos(\theta_i - \theta_j) \approx 1 - \frac{(\theta_i - \theta_j)^2}{2} \tag{24}$$

The transmission loss in (23) becomes,

$$\Psi_{ij} \approx \frac{3R_{ij}V^2(\theta_i - \theta_j)^2}{R_{ij}^2 + X_{ij}^2} \tag{25}$$

Finally, using the same assumption as in (18) and plugging in the active power in (19), the transmission loss becomes

$$\Psi_{ij} \approx \frac{R_{ij}}{3V^2}P_{ij}^2 = R_{ij}^{\text{PU}}P_{ij}^2 \tag{26}$$

where R_{ij}^{PU} is the per unit resistance of the line between bus i and j (under the same assumption of a flat, 1 p.u. voltage profile at all buses).

To retain the linear nature of the optimization problem, we approximate the quadratic term in (26) with a set of linear inequality constraints, similar to the approach in [31]. First, the linearized transmission loss on line l at time step t is defined as a non-negative variable ψ_{lt} (therefore setting the lower limit):

$$\psi_{l,t} \geq 0 \tag{27}$$

Second, the upper limit to ψ_{lt} is assigned according to the maximum power flow of the line F_l from Eq. (26),

$$\psi_{l,t} \leq R_l^{\text{pu}}F_l^2 \tag{28}$$

These upper and lower limits must be complemented by additional constraints, which have the key purpose of giving ψ_{lt} a more realistic value. In general terms, this can be done by tightening the loss relaxation between 0 and the maximum power flow (note that the constraints are mirrored as the power flow can take both positive and negative values):

$$\psi_{l,t} \geq m_v f_{l,t} + a_v \qquad \forall v = 1, 2, \ldots, w \tag{29}$$

$$\psi_{l,t} \geq -m_v f_{l,t} + a_v \qquad \forall v = 1, 2, \ldots, w \tag{30}$$

where w is the total number of segments used in the loss approximation. The terms m_v and a_v can now be found using two different approaches.

Here we substitute the two buses i and j with the connecting AC transmission line l. One is using the tangents of the quadratic function (26) as in [12]. The transmission loss at the end of segment v is calculated as

$$\Psi_l(v) = R_l^{\text{pu}}(\frac{v}{n}F_l)^2 \qquad \forall v = 1, 2, \ldots, w \tag{31}$$

Then the slopes and intercepts describing each of the linear segments are:

$$m_v = \frac{\mathrm{d}\Psi_l}{\mathrm{d}P_l}\Big|_{P_l = \frac{v}{n}F_l} = \frac{2v}{n}R_l^{\text{pu}}F_l \qquad \forall v = 1, 2, \ldots, w \tag{32}$$

$$a_v = \Psi_l(v) - m_v\frac{v}{w}F_l \qquad \forall v = 1, 2, \ldots, w \tag{33}$$

One problem with using the tangents is that, for small v, it either leaves a region of lossless flows or it allows for a small loss at high flow, as illustrated in Fig. 2. In the second approach, the tighter lower bound can be identified by connecting the points on the quadratic function. The slope in (32) turns into

$$m_v = \frac{n[\Psi_l(v) - \Psi_l(v-1)]}{F_l} = \frac{(2v-1)R_l^{\text{pu}}F_l}{w} \qquad \forall v = 1, 2, \ldots, w \tag{34}$$

while the offset can still be calculated using Eq. (33).

2.4. Generator: cluster unit commitment with minimum output

The cluster commitment depicts the on/off status of a set of generator units. We consider that a power plant has identical units, whose commitments are clustered together, as shown in [32,33]. The unit commitment logic is given by

$$u_{k,t} - u_{k,t-1} = y_{k,t} - z_{k,t} \quad \forall k \in \mathcal{K}^{\text{thermal}}, t \in \mathcal{T} \tag{35}$$

where $u_{k,t}$ is the number of units which are on during a given time interval, $y_{k,t}$ the number of units starting up and $z_{k,t}$ the number of units shutting down. For the generator power output, Gentile et al. [34] provides the tightest representation, as follows. The power output above minimum $\hat{e}^{\text{output}}$ is

$$\hat{e}_{k,t} \leq (E_k - \underline{E}_k)u_{k,t} - (E_k - \text{SD}_k)z_{k,t+1} - \max(\text{SD}_k - \text{SU}_k, 0)y_{k,t} \quad \forall k \in \mathcal{K}^{\text{thermal}} | \text{TU}_k = 1, t \in \mathcal{T} \tag{36}$$

$$\hat{e}_{k,t} \leq (E_k - \underline{E}_k)u_{k,t} - (E_k - \text{SU}_k)y_{k,t} - \max(\text{SU}_k - \text{SD}_k, 0)z_{k,t+1} \quad \forall k \in \mathcal{K}^{\text{thermal}} | \text{TU}_k = 1, t \in \mathcal{T} \tag{37}$$

$$\hat{e}_{k,t} \leq (E_k - \underline{E}_k)u_{k,t} - (E_k - \text{SU}_k)y_{k,t} - (E_k - \text{SD}_k)z_{k,t+1}$$

$$\forall k \in \mathcal{K}^{\text{thermal}} | \text{TU}_k > 1, t \in \mathcal{T} \tag{38}$$

where $\hat{e}_{k,t}$ is the power output above the minimum, E_k and $\underline{E}_k$ the capacity and minimum level of power output, respectively. SD_k and SU_k are the power outputs when a unit is shutting down and starting up, respectively. TU_k is the minimum uptime. The total power output for a given unit and time interval is:

$$e^{\text{output}}_{k,t} = \underline{E}_k u_{k,t} + \hat{e}_{k,t} \quad \forall k \in \mathcal{K}^{\text{thermal}}, t \in \mathcal{T}. \tag{39}$$

2.5. Generator: minimum up and down times

Once started up, a thermal generator needs to stay on for a certain amount of time before proceeding to shut down, and vice versa. Following [34], we realize the minimum up and down time constraints of a generator unit with

$$\sum_{i=t-\text{TU}_k+1}^{t} y_{k,i} \leq u_{k,t} \quad \forall k \in \mathcal{K}^{\text{thermal}}, t \in [\text{TU}_k, |\mathcal{T}|] \tag{40}$$

$$\sum_{i=t-\text{TD}_k+1}^{t} z_{k,i} \leq (A_k + \alpha_k) - u_{k,t} \quad \forall k \in \mathcal{K}^{\text{thermal}}, t \in [\text{TD}_g, |\mathcal{T}|] \tag{41}$$

where TD_k is the minimum down time, A_k is the number of initially installed units and α_k is the number of additionally invested units. Finally, T is the total number of time steps.

2.6. Generator: start-up and shut-down trajectories

In more detailed energy system optimization models, it is possible to consider the power output during the start-up and shut-down processes by applying the formulation given by [35]. In this case, the simple expression in (39) is replaced by:

$$e^{\text{output}}_{k,t} = \sum_{i=1}^{\text{SUD}_k} E^{\text{SU}}_k y_{k,(t-i+\text{SUD}_k+1)} + \sum_{i=1}^{\text{SDD}_k} E^{\text{SD}}_k z_{k,t-i+1} + \underline{E}_k u_{k,t} + \hat{e}_{k,t}$$
$$\forall k \in \mathcal{K}^{\text{thermal}}, t \in \mathcal{T} \tag{42}$$

where SUD_k and SDD_k are the start-up and shut-down durations. E^{SU}_k and E^{SD}_k are the corresponding power outputs over the start-up and shut-down trajectories.

2.7. Generator: ramp rate limit

The ramp rate denotes the speed with which a generator can change its production over a given time interval. The ramp rate constraints reflect the dynamics of thermal processes inside a unit and are given by [14]:

$$\hat{e}_{k,t} - \hat{e}_{k,t-1} \leq RU_k E_k u_{k,t} \qquad \forall k \in \mathcal{K}^{\text{thermal}}, t \in \mathcal{T} \tag{43}$$

$$-\hat{e}_{k,t} + \hat{e}_{k,t-1} \leq RD_k E_k u_{k,t} \qquad \forall k \in \mathcal{K}^{\text{thermal}}, t \in \mathcal{T} \tag{44}$$

where RU_g and RD_g are the maximum ramp-up and ramp-down rates.

3. Case studies, implementation and solution feasibility test

In this paper, we formulate and compare energy system design and operation planning problems. As shown in Fig. 1, we consider two overarching case studies: the electric-only IEEE 118-bus test system (IEEE 118-Bus) and the multi-energy, zero-emission NL with electricity and hydrogen (NL-8-Node). The transmission network of IEEE 118-Bus is pre-determined, while NL-8-Node is a greenfield design exercise, meaning that there are consumption/generation nodes defined, but they are not linked by pre-existing infrastructure. In both cases, we implement the formulations presented in Section 2. Then we will evaluate the necessity of each characteristic by removing it from the complete formulation. Before that, we explain in this section the optimization objectives of the two cases and additional descriptions of the technologies, in the separate Sections 3.1 and 3.2.

3.1. IEEE 118-bus test system

To examine the importance of modeling the transmission network and generation flexibility characteristics for a power-only (electricity) system application, we introduce the IEEE 118-Bus test system, which features 118 buses linked by 186 AC transmission lines, as shown in Fig. 3 [36]. The test case was adapted to a generation expansion planning problem in [14]. With the data imported from [14], the problem has a time horizon of 24 h. While this time frame is short, it is sufficient for our purposes, as the focus is on the differences in system design rather than the design itself.

The network is characterized by 91 loads, 10 fast-start open-cycle gas turbine (OCGT) plants, and 54 slow-start thermal plants using gas (combined-cycle), coal, or oil. Additionally, there are 3 types of energy storage systems, namely pumped hydro storage (PHS), compressed air energy storage (CAES), and electric battery. 3 buses come with wind power, with pre-determined capacities, 1272 MW in total. The total average load of the system is 3578.6 MW, with a peak of 5117.5 MW. Regarding further detailed data of this case, we refer readers to [14].

In this case, the transmission network is predetermined. Therefore, the optimization aims at minimizing the sum of investment and linear operational costs of technologies, and of start-up costs of thermal generators, given as

$$\min \sum_{k \in \mathcal{K}} \left[C^{\text{I}}_k \alpha_k + \sum_{t \in \mathcal{T}} C^{\text{O}}_k e^{\text{output}}_{k,t} \right] + \sum_{k \in \mathcal{K}^{\text{thermal}}} \sum_{t \in \mathcal{T}} C^{\text{SU}}_k y_{k,t} \tag{45}$$

where C^{I}_k is the investment cost per unit capacity. C^{O}_k is the linear operational cost per unit output. C^{SU}_k is the start-up cost of thermal generators. α_k is the invested capacities. Lastly, $\mathcal{T}$ is the set of time steps.

3.2. Multi-energy zero-emission NL (electricity+hydrogen)

The multi-energy system application is a self-sufficient, zero-emission national energy system designed for the Netherlands, considering two energy carriers, electricity and hydrogen. Compared to the IEEE 118-Bus test system described in Section 3.1, here we conduct greenfield investments of renewable energy technologies, hydrogen technologies, and the transport infrastructure. We envisage that, due to decarbonization policy, no thermal plants other than nuclear are allowed to be built. The dataset of this case can be found in [37].

This case is adapted from [38], and consists of 8 geographical nodes, of which 3 are off-shore and 5 on-shore, as shown in Fig. 4. The geographical nodes are named after their relative positions, each representing an area in the Netherlands and its exclusive economic zone in the North Sea, on which the technologies can be built. The dashed lines indicate potential electricity and hydrogen transmission (pipe)lines. The distances of the connections are listed in Table A.1. The transmission network is co-optimized as part of the problem. The objective is then as in (45) plus the investment cost and fixed operation and maintenance cost of transmission lines,

$$\min \sum_{k \in \mathcal{K}} \left[C^{\text{I}}_k \alpha_k + \sum_{t \in \mathcal{T}} C^{\text{O}}_k e^{\text{output}}_{k,t} \right] + \sum_{k \in \mathcal{K}^{\text{thermal}}} \sum_{t \in \mathcal{T}} C^{\text{SU}}_k y_{k,t} + \sum_{l \in \mathcal{L}} C^{\text{I}}_l \alpha_l \tag{46}$$

where $\mathcal{K}$ is the set of conversion (including generation) and storage technologies, namely solar photovoltaic (PV) panels, wind turbines, electrolyzers and fuel cells, nuclear plants, electric battery, and hydrogen tank. $\mathcal{L}$ is the set of energy transmission lines for both electricity

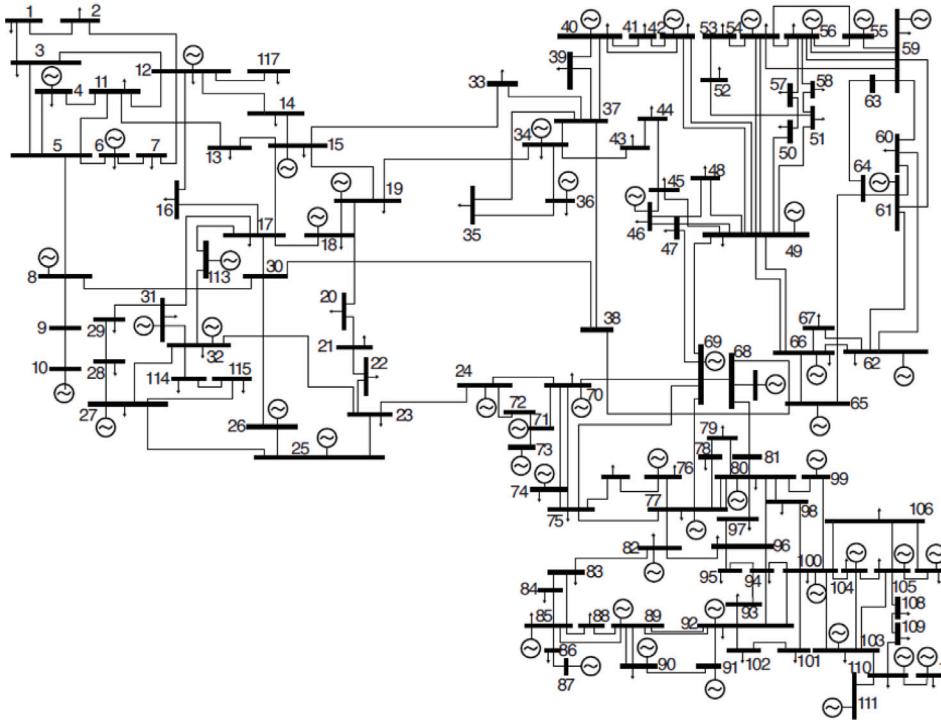

Fig. 3. Topology of the IEEE 118-Bus test system, adapted from [36]. Wind turbines are located at buses 33, 69 and 77.

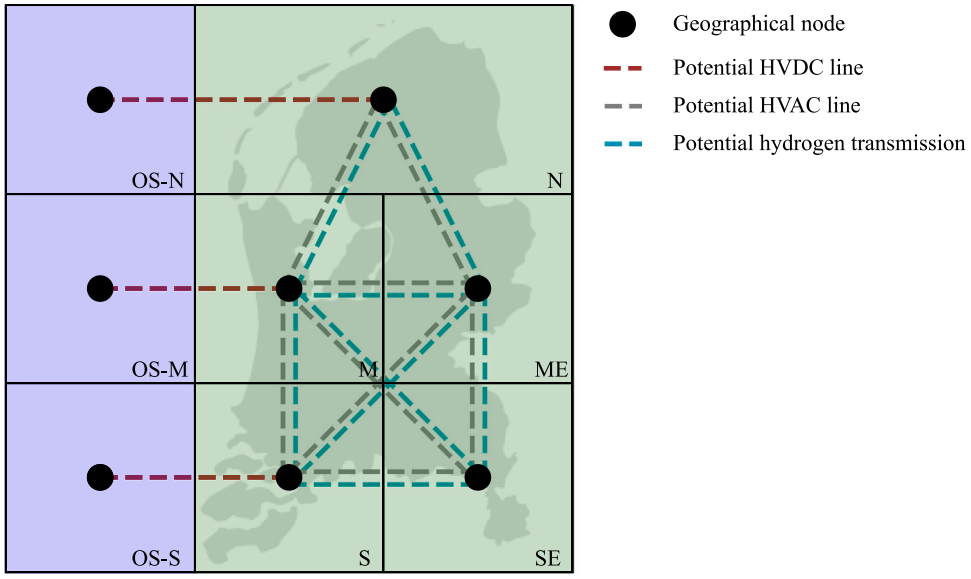

Fig. 4. Topology of the zero-emission NL 8-Node case study.

and hydrogen. To align with the basic formulation in Section 2.1.2, the invested capacities of technologies that are discretely invested take into account the unit capacity and the discrete investment decisions.

$$\alpha_l = F_l d_l \qquad \forall l \in \mathcal{L}^{\mathrm{AC}} \tag{47}$$

$$\alpha_k = E_k d_k \qquad \forall k \in \mathcal{K}^{\mathrm{thermal}} \tag{48}$$

For this case, we derive the investment cost parameters from referenced data. The fixed operation and maintenance cost, and the net present value of the annualized investment cost are given by

$$C_l^{\mathrm{I}} = \frac{\tilde{C}_l^{\mathrm{I}} L_l}{Y_l} \mathrm{NPV}_l (1 + \mathrm{FOM}_l) \qquad \forall l \in \mathcal{L} \tag{49}$$

where $\tilde{C}_l^{\mathrm{I}}$ is the investment cost per MW per km of the line, Y_l the product design lifetime, NPV_l the net present value ratio of the investment, and FOM_l the annual fixed operation and maintenance cost ratio. We assume a lifetime of 40 years for all line types. Table A.2 shows other relevant economic parameters. Similarly, we consider for energy conversion (including generation) and storage technologies the net present value investment cost together with the fixed operation and maintenance cost, given as

$$C_k^{\mathrm{I}} = \frac{\tilde{C}_k^{\mathrm{I}}}{Y_k} \mathrm{NPV}_k (1 + \mathrm{FOM}_k) \quad \forall k \in \mathcal{K} \tag{50}$$

where $\tilde{c}_k^I$ is the investment cost per kW. The economic parameters of these technology types are listed in Table A.7. The net present value is

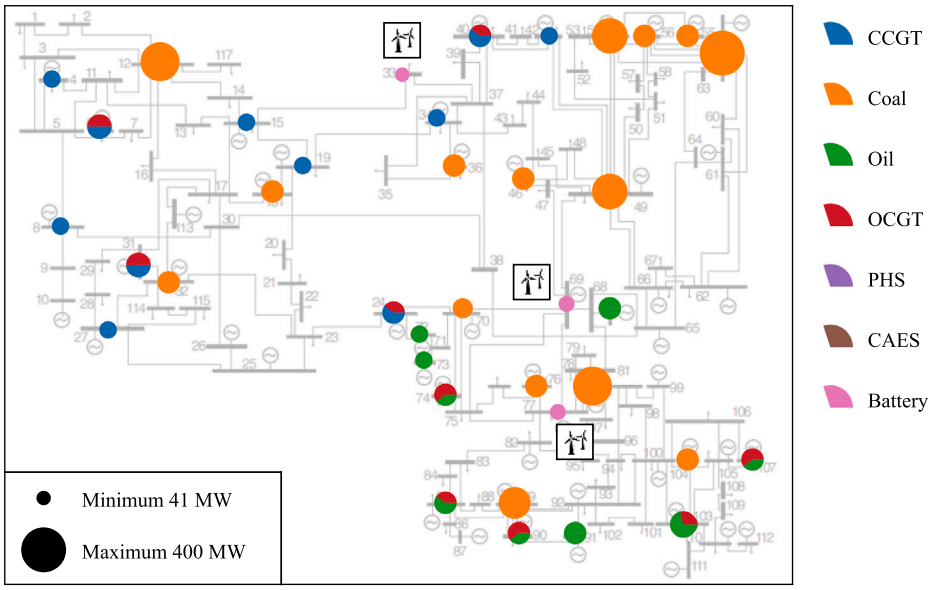

Fig. 5. IEEE 118-Bus test system capacity design; reference model.

calculated as

$$\mathrm{NPV}_i = \frac{(1+\mathrm{DF})^{Y_i}-1}{Y_i \mathrm{DF}} \quad \forall i \in \mathcal{L} \cup \mathcal{K} \tag{51}$$

where DF is the discount factor used throughout this case study. We assume it to be 0.04.

3.2.1. Energy transport infrastructure

Between on-shore nodes, we allow building high-voltage alternating current (HVAC) electricity lines. For these lines, due to the level of abstraction we adopt and the non-linearity between the line capacity and its reactance, we consider only one standard line type with a capacity of 1698 MVA [39]. We make effective the transmission characteristics in (19) and (27) - (34) with the line properties in Table A.3, where the $\bar{R}$ and $\bar{X}$ are the resistance and reactance per unit distance. We then compute the line resistance and reactance as their product with the corresponding distances. Discrete investment decisions of this line type can be made, as given by (4).

As for the HVDC lines connecting off-shore nodes to nearby on-shore nodes, we assume a fixed loss factor of 2%, aligned with reported numbers [40]. As there is only one-directional flow from offshore to onshore, we have equality constraints,

$$\psi_l = \beta_l f_{l,t} \qquad \forall l \in \mathcal{L}^{\mathrm{DC}} \tag{52}$$

where ψ_l is the loss, β_l is the above-mentioned loss factor (2%) and f_{lt} the electricity flow in the HVDC line.

The transportation of hydrogen is only allowed onshore via dedicated hydrogen pipelines. In order to compensate for pressure drops, hydrogen pipelines require energy to sustain recompressions along the line. We assume for this a linear relationship, and that the energy is provided by using part of the hydrogen transported (similarly as in natural gas networks). The loss is then given by

$$0 \le \psi_l \le \beta_l F_l \qquad \forall l \in \mathcal{L}^{\mathrm{H_2}} \tag{53}$$

$$\psi_l \ge \beta_l f_{l,t} \qquad \forall l \in \mathcal{L}^{\mathrm{H_2}}, t \in \mathcal{T} \tag{54}$$

$$\psi_l \ge -\beta_l f_{l,t} \qquad \forall l \in \mathcal{L}^{\mathrm{H_2}}, t \in \mathcal{T} \tag{55}$$

where $\mathcal{L}^{\mathrm{H_2}}$ is the set of hydrogen pipelines. β_l is the loss coefficient of the hydrogen pipeline, equal to 3.3E−5 (adopted from [41]). In our study, we use 5 GW for the maximum capacity $\overline{F}_l$ of hydrogen pipelines, which fits in the range of 1 to 13 GW proposed in the European Hydrogen Backbone report [42].

3.2.2. Renewable energy technologies

For solar photovoltaic (PV) panels and wind turbines that require large areas, we consider the limits in the land and sea resources, listed in Table A.4. The solar area is the total available rooftop area distributed by the amount of built-up area on each node [43]. The on-shore and off-shore wind areas are decided by evaluating the installed capacities [44] and official plans for wind energy development in the Netherlands [45].

Accordingly, the installed capacity of solar panels is limited by their potential

$$0 \le \alpha_k \le \eta_k I^{\mathrm{STC}} \mathrm{SA}_{n(k)} \quad \forall k \in \mathcal{K}^{\mathrm{solar}} \tag{56}$$

where η_v is the assumed constant PV efficiency. Here, we use 0.22, which reflects the average level of current solar PV technologies [46]. I^{STD} is the irradiance at standard test condition, 1000 W/m^2. $\mathrm{SA}_{b(v)}$ is the solar area of the node, at which the PV panel is located. The power output from the PV panel is dependent on the solar irradiance:

$$0 \le e^{\mathrm{output}}_{k,t} \le \eta_k I_{n(k),t} \alpha_k \quad \forall k \in \mathcal{K}^{solar}, t \in \mathcal{T} \tag{57}$$

where $I_{n(k),t}$ is the solar irradiance of the node $n(k)$ at time step t. Curtailment of PV panel power output is allowed.

Similarly, the capacity of wind turbines is installed within the potential of their designated area,

$$0 \le \alpha_k \le \frac{E^0_k}{\mathrm{WA}^0} \mathrm{WA}_{n(k)} \quad \forall k \in \mathcal{K}^{\mathrm{wind}} \tag{58}$$

where E^0_k is the unit power capacity of the wind turbine. WA^0_k is the average area per turbine. And $\mathrm{WA}_{n(k)}$ is the area for wind turbines at the node where the wind turbines are built. We assume that wind turbines are placed on the vertices of squares. Therefore, WA^0 is the square of the distance between two turbines. We use 400 m here, which is aligned with practice when building wind farms [38,47]. We also allow curtailment of the power output, which is limited by the available power

$$0 \le e^{\mathrm{output}}_{k,t} \le E^{\mathrm{avail}}_{k,t} \alpha_k \quad \forall k \in \mathcal{K}^{\mathrm{wind}}, t \in \mathcal{T} \tag{59}$$

where $E_{k,t}^{\text{avail}}$ is the available wind power, derived from the wind speed as

$$E_{k,t}^{\text{avail}} = \begin{cases} 0 & \text{if } V_{n(k),t} < V_k^{\text{cut-in}} \\ \frac{V_{n(k),t}^3 - V_k^{\text{cut-in3}}}{V_k^{\text{rated3}} - V_k^{\text{cut-in3}}} & \text{if } V_k^{\text{cut-in}} \le V_{n(k),t} \le V_k^{\text{rated}} \\ 1 & \text{if } V_k^{\text{rated}} < V_{n(k),t} \le V_k^{\text{cut-out}} \\ 0 & \text{otherwise} \end{cases} \quad \forall k \in \mathcal{K}^{\text{wind}}, t \in \mathcal{T} \tag{60}$$

where $V_k^{\text{cut-in}}$, V_k^{rated} and $V_k^{\text{cut-out}}$ are the design cut-in, rated and cut-out wind speed of the wind turbine, respectively. The values we use for both on-shore and off-shore wind turbines are listed in Table A.5. $V_{n(k),t}$ is the wind speed at hub height. This is converted from the wind speed data using the 1/7th power law [48],

$$V(h) = V(h^0)(\frac{h}{h^0})^{1/7} \tag{61}$$

where h^0 is the reference height of 10 m at the meteorological measurement [49]. The hub height of 123 m is taken from the average of available turbine models [38].

3.2.3. Hydrogen technologies

We include electrolyzers and fuel cells for the conversion between electricity and hydrogen in the on-shore nodes. The electrolyzers convert water to hydrogen and oxygen upon electricity provision, while fuel cells operate in the other way round. Their energy output is limited by the decision variable of installed capacity α_κ,

$$0 \le e_{k,t}^{\text{output}} \le \alpha_k, \quad \forall k \in \mathcal{K}^{\text{EC}} \cup \mathcal{K}^{\text{FC}}, t \in \mathcal{T} \tag{62}$$

where $\mathcal{K}^{\text{EC}}$ and $\mathcal{K}^{\text{FC}}$ are the sets of hydrogen electrolyzer and fuel cells, respectively. Their energy conversion is then

$$e_{k,t}^{\text{output}} = \eta_k e_{k,t}^{\text{input}} \quad \forall k \in \mathcal{K}^{\text{EC}} \cup \mathcal{K}^{\text{FC}}, t \in \mathcal{T} \tag{63}$$

where $e_{k,t}^{\text{input}}$ is the energy input and η_k is the conversion efficiency. We use 0.58 for fuel cells [50] and 0.8 for electrolyzers [51].

3.2.4. Nuclear plants

To include dispatchable electricity generation plants while adhering to a net-zero emissions system, we consider nuclear plants. More specifically, we allow a potential of 4×1570 MW nuclear plants at the S node, where Borssele, the current nuclear power plant is located [52,53]. Regarding the dynamic behaviors of the nuclear plant, we apply the generator characteristics in Eq. (35) - (44). The parameters are given in Table A.6.

3.2.5. Energy storage technologies

We include the possibility of adding Li-ion batteries for electricity storage, depicted in Eq. (8) and (12). We assume a round-trip efficiency η_s of 0.95, which is close to the reported values [54]. We use the value 1E-4 as the self-dissipation rate σ_s here, according to [55]. And the energy-to-power ratio EPR_s is 4.

For hydrogen storage, we assume no hydrogen loss during the charging and storage processes. And an energy-to-power ratio of 3 is applied. However, we take into consideration the compression work to pressurize gaseous hydrogen for storage, given as

$$\tilde{e}_{k,t}^{\text{input}} = \epsilon_k c_{k,t} \quad \forall k \in \mathcal{K}^{\text{H}_2\text{storage}}, t \in \mathcal{T} \tag{64}$$

where ϵ_k is the ratio of compression work to the energy content of hydrogen stored. We use 5%, in accordance with [56]. $\tilde{e}_{k,t}^{\text{input}}$ is the compression work. The compression work is counted in the form of electricity consumption by the technology.

3.3. Implementation

The models for the two case studies are implemented using *Pyomo* [57] in Python, while the optimization problems are solved with *Gurobi 10* [58] on a personal computer that runs on AMD Ryzen 7 4800H CPU with 16 GB of RAM. The RAM capacity is not exceeded for any of the cases.

We use two ways to solve the two cases, as their complexity differs drastically. The IEEE 118-Bus case can be solved directly. Whereas to run the case study of self-sufficient zero-emission NL with hydrogen in a reasonable amount of time, we couple the time steps in 4 design weeks, instead of using a full-year horizon, similar to the approach put forward in [17]. We use design weeks because the operation cycles of the nuclear plants can exceed 24 h.

3.4. Feasibility test

Aside from examining the direct solution outcomes, we evaluate the solution quality of the simplified cases by conducting a feasibility test on the decision variables concerning capacities for the energy transport, conversion and storage technologies. The feasibility test is done by fixing the technology capacities, as provided by the optimal solution of a simplified case, and formulating the optimization problem with the reference case, which has the most detailed set of power system characteristics. Note that this is not the same concept as the feasibility of optimization solutions. The feasibility test, therefore, demonstrates whether the simplified case would provide a system design that is likely feasible to operate in reality. A negative result reveals defects in the simplified case, even though it could be close to the more detailed reference case in the other metrics mentioned above.

4. Results and discussion

In this section, we discuss the implications of different modeling approaches in energy system optimization. First, we present the results of the IEEE 118-Bus electricity-only system, where we solve a generation and storage capacity expansion planning problem. Second, we discuss the multi-energy system, a more complex, greenfield design involving generation, storage and transmission planning of a zero-emission system for the Netherlands. The purpose of having these two case studies is to examine the need for modeling the characteristics that are commonly considered in the power system literature, in both electricity-only and multi-energy applications. To identify the combination of the energy system application and the characteristics conveniently, we define an abbreviation code, which consists of a prefix and a suffix, as listed in Table 1. The prefix represents the energy system application. The suffix denotes the combination of network and generator characteristics. By "unit commitment" in the table, we refer to the set of characteristics consisting of clustered unit commitment, minimum up and down time, and start-up and shut-down trajectories. For the AC loss, the numeric codes, such as "10P" and "3P", tell the number of pieces used in the piece-wise linearization of the quadratic loss. And "connect" or "tangent" means the linearization approach, as provided in Eq. (27)–(34).

4.1. System capacity design

4.1.1. IEEE 118-bus test system

The results of the optimal system capacity designs of the IEEE 118-Bus are displayed in Fig. 6. The capacities of technologies at each bus are depicted with pies, where each color represents a specific technology, and the size corresponds to the design capacity. It is important to note that, in this case, the power generation from wind turbines is predetermined and therefore not a part of the optimization problem. To convey an understanding of the interactions among generation and storage technologies, we illustrate their locations in the figure.

Table 1
Prefixes and suffixes denoting the combination of energy systems and modeling characteristics.

Prefix	Case				Relevant equations
IEEE-	IEEE 118-Bus test system				(1)–(12) (45)
NL8-	Self-sufficient zero-emission NL with hydrogen				(1)–(12) (46)–(64)
Suffix	AC power transmission		Thermal generator		Relevant equations
	Transport model	Loss	Ramp rate limit	Unit commitment	
-ref	KVL	10P connect	✓	✓	(21) (27)–(30) (33)–(44)
-EB	Energy balance	10P connect	✓	✓	(27)–(30) (33)–(44)
-lossless	KVL	lossless	✓	✓	(21) (35)–(44)
-free_ramp	KVL	10P connect	✗	✓	(21) (27)–(30) (33)–(42)
-free_unit	KVL	10P connect	✓	✗	(21) (27)–(30) (33)–(34) (43) (44)
-3Pconnect	KVL	3P connect	✓	✓	(21) (27)–(30) (33)–(44)
-2Pconnect	KVL	2P connect	✓	✓	(21) (27)–(30) (33)–(44)
-1Pconnect	KVL	1P connect	✓	✓	(21) (27)–(30) (33)–(44)
-3Ptangent	KVL	3P tangent	✓	✓	(21) (27)–(30) (33)–(44)
-2Ptangent	KVL	2P tangent	✓	✓	(21) (27)–(30) (33)–(44)
-1Ptangent	KVL	1P tangent	✓	✓	(21) (27)–(30) (33)–(44)

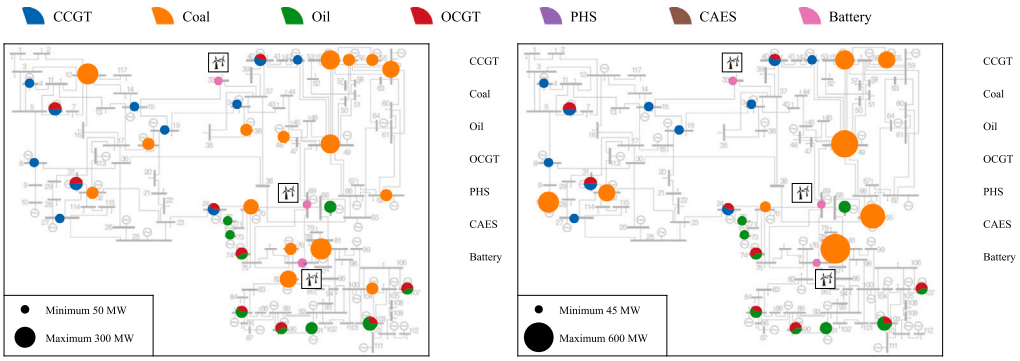

(a) IEEE-EB - excluding KVL from the reference model. (b) IEEE-lossless - excluding AC transmission losses from the reference model.

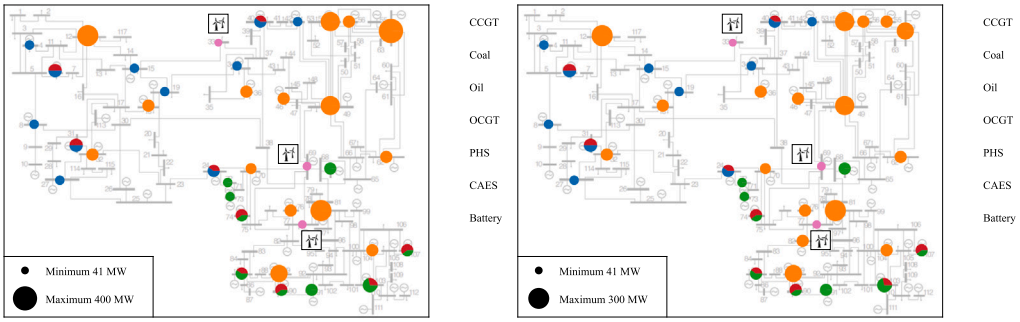

(c) IEEE-free_ramp - excluding ramp rate limits from the reference model. (d) IEEE-free_unit - excluding unit commitment characteristics from the reference model.

Fig. 6. IEEE 118-Bus test system generation and storage planning with different characteristic combinations.

The IEEE-ref in Fig. 5 provides the foundation for evaluating the need for each characteristic. In this reference case, the system is predominantly powered by coal-firing power plants, with larger units being constructed. In contrast, the capacity of combined-cycle gas turbines (CCGT), open-cycle gas turbines (OCGT) and oil-firing plants is smaller and more dispersed. Notably, battery units are deployed at the buses where wind power is injected into the system, likely to mitigate the fluctuating generation. Pumped hydro storage (PHS) and compressed air energy storage (CAES) units are absent in this solution.

Fig. 6(a) shows the solution when we model the transport network via the energy balance alone, thus omitting the electric circuit theory constraints (KVL). Without KVL, the power flow on each line becomes less dependent on the others. One consequence is the replacement of large generators by smaller ones. The capacity of the large coal-firing generator at bus 59, situated at the top right in the figures, is significantly reduced from 400 MW to 200 MW. Simultaneously, another coal-firing generator is added at bus 62, center-right in the figure, and additional coal-firing units emerge at bus 70, located around the center. Examining the lower center of the figure, we observe that the coal-firing generator capacity at bus 89 is transferred to bus 82, moving from a bus with no local demand to one that has demand. We attribute this to the avoidance of losses in inter-nodal power transmission, made possible by removing the KVL constraints.

Moreover, the removal of KVL can increase the need for energy storage. At bus 77 in Fig. 6(a), an extra PHS unit appears compared to the reference case. We interpret this as an indication that, when

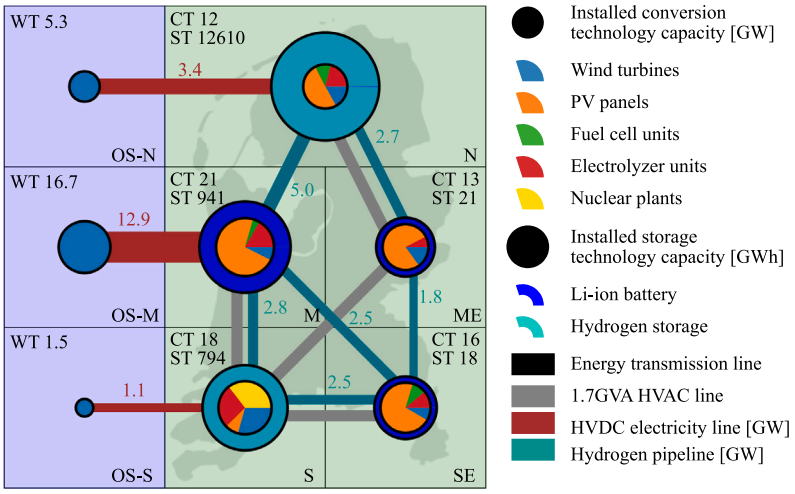

Fig. 7. NL-8-Node system capacity design; reference model. Summed capacities of wind turbines (WT), conversion technologies (CT), and storage technologies (ST) are indicated on each node in GW.

the power flow is not constrained by KVL, storage can function more effectively in storing and distributing energy from other buses.

The solution of the lossless IEEE 118-Bus, presented in Fig. 6(b), deviates significantly from the reference case. In contrast to IEEE-EB, the lossless version exhibits more concentrated capacities for coal-firing power plants. The generators at 9 buses (12, 18, 36, 46, 56, 59, 76, 89 and 104) are replaced by larger units at 5 buses: 10, 32, 49, 65 and 80. Upon reviewing the input data, it becomes evident that both the investment and operation costs of the new units are lower. This suggests that avoiding transmission losses in the reference case (where losses are modeled in more detail) compensates for the more expensive locally distributed generation.

As for IEEE-free_ramp, where the thermal generators can ramp up or down freely, we observe in Fig. 6(c) the relocation of the coal-firing generator from bus 55 in the reference case to bus 62. These two generators have identical investment and generation costs. There is an electricity demand with a peak of 875 MW from buses 54–60 and at bus 62, there is an additional demand with a peak of 106 MW. Therefore, disregarding the ramp rate limits allows the three generators at buses 54, 56 and 59 (without the one at bus 55) to meet the demand in that area. The generator is placed at bus 62 instead, to satisfy local demand without incurring any transmission loss. In general, we consider the impact of removing the ramp rate limits to be small in the IEEE 118-Bus test system.

Similarly, when the unit commitment constraints are excluded from the problem, as shown in Fig. 6(d), a 200 MW coal-firing generator capacity is removed from bus 59, and an extra 100 MW is installed at bus 62 in the optimal solution. This demonstrates that the 200 MW capacity at bus 59 is needed in the reference case because of the unit commitment and its constraints on the power output, as well as the minimum up and down periods. Removing the unit commitment constraints leads to an underestimation of the required capacity. The smaller generator at bus 62 is therefore introduced to fulfill the local demand.

In conclusion, for the IEEE 118-Bus test system, network characteristics play a more significant role in determining generation and storage expansion capacities than the generator flexibility characteristics. The application of KVL when modeling the network flows limits the dispersion of generator capacity, while the presence of transmission losses enhances the value of local generation. The ramp rate limit and unit commitment constraints delineate the generators' flexibility. Dropping either of the two leads to some underestimation of the optimal generator capacity.

4.1.2. NL-8-node

The result of the optimal system capacity design for the NL-8-Node using the reference model is pictured in Fig. 8, based on the nodal configuration outlined in Fig. 4. Energy conversion technologies (CT), including wind turbines (WT), PV panels, fuel cells, electrolyzers and nuclear plants are illustrated with a pie chart at each node. The annulus surrounding the pie represents the system design of storage technologies (ST), namely Li-ion battery (light blue) and hydrogen storage (light blue). The sum values of CT and ST, or WT on the off-shore nodes are provided at the top corners of each node in GW. Transmission lines between nodes are illustrated, and capacities of HVDC lines and hydrogen pipelines are indicated in the nearby annotations.

In the optimal system design for NL8-ref in Fig. 7, conversion and storage technology capacities are reasonably distributed across the eight nodes. On the three off-shore nodes, wind turbines are installed at the full capacities allowed by the spatial constraints due to their high capacity factor. Connections from offshore nodes to onshore are smaller than the wind turbine capacities, which is explainable given that the available wind power is not always at peak generation capacity. Therefore, building extra connection capacity has a diminishing value for the objective of minimizing total system cost.

Moving to the onshore nodes, the capacities of conversion technologies align with the distribution of energy demands. Node M, with the largest electricity demand, has the highest power generation capacity. Node S hosts a substantial number of electrolyzer units to meet the local hydrogen demand due to industrial electrification. Most hydrogen storage is located at node N, the only node where salt caverns are available for hydrogen storage.

Concerning the onshore energy transmission networks in the reference case, each node is connected to at least two hydrogen pipelines. However, with the exception of node S, all nodes have a single AC electricity connection, and notably, no electrical loops are formed. This is due to the inclusion of KVL for HVAC lines. Defining the flow by voltage angles prevents the formation of cycles, allowing the electricity to flow freely within the line capacity. Otherwise, if we have cycles, extra local generation capacity could be needed as the AC flows in different lines will become interdependent, and therefore, transport less.

Fig. 8(a) shows that, indeed, when KVL is ignored, cycles in the electricity network are constructed. The flows are now free to vary within the capacities, leading to considerably fewer conversion and storage technologies at nodes M, ME and S. Hydrogen storage at node N increases significantly, taking further advantage of the cost-effective salt caverns. Furthermore, the absence of KVL strengthens the role

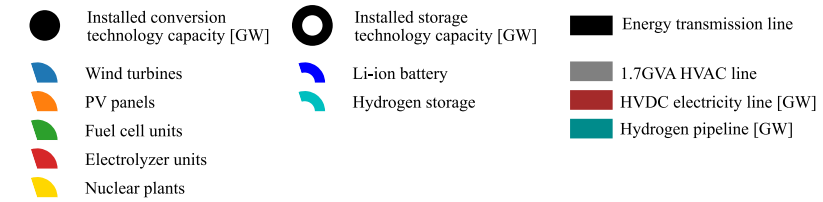

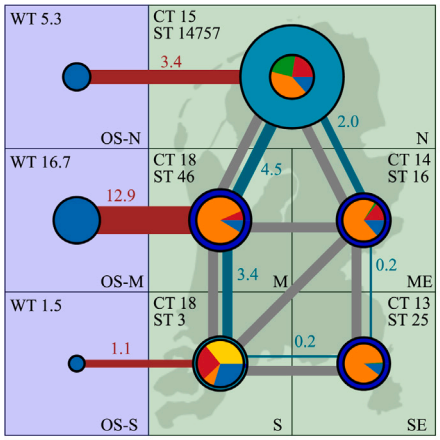

(a) NL8-EB - excluding KVL from the reference model.

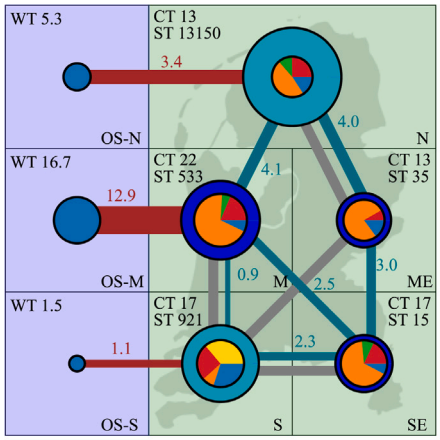

(b) NL8-lossless - excluding AC transmission from the reference model.

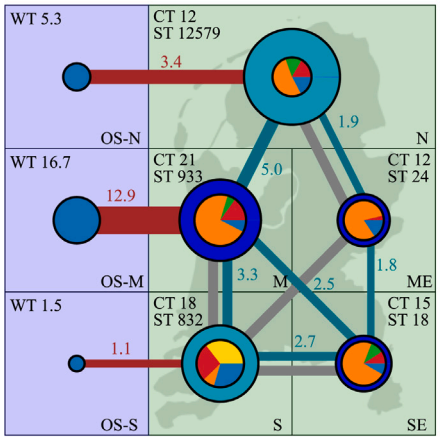

(c) NL8-free_ramp - excluding ramp rate from the reference model.

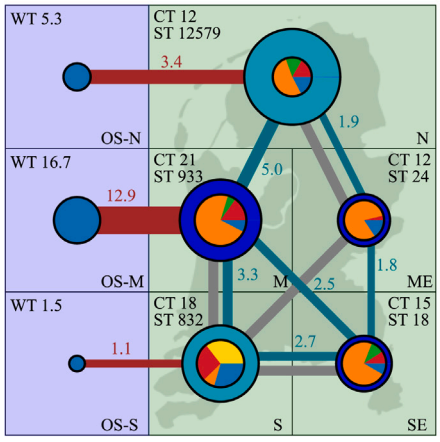

(d) NL8-free_unit - excluding unit commitment characteristics from the reference model.

Fig. 8. NL-8-Node system transmission, conversion (including generation) and storage planning with different characteristic combinations. Summed capacities of wind turbines (WT), conversion technologies (CT), and storage technologies (ST) are indicated on each node in GW.

of electricity in the energy transmission infrastructure. Compared to the reference, the hydrogen network of NL8-EB is reduced. Both the fuel cell and electrolyzer units at node N are larger, indicating that without KVL, more electricity is converted to hydrogen for storage, and more hydrogen is converted back to electricity for transmission to other nodes. However, such under-planning of the capacities is not feasible, as discussed in Section 4.2.

Transmission losses bring implicit costs to energy transport. When overlooked, the optimal solution tends to favor remote, yet more cost-effective generation. In the NL8-lossless case shown in Fig. 8(b), the battery storage capacity at node M significantly decreases, with mild increases in hydrogen storage capacities at nodes N and S. By contrast, energy conversion technology capacities and transmission networks do not vary much from the reference case. Compared with NL8-EB in Fig. 8(a), this means transmission losses have a lesser impact on system capacity design than KVL.

On the other hand, generator characteristics do not influence the system capacity design for the NL-8-Node system, as visible in Figs. 6(c) and 6(d). The reason is that, in this system, the generator characteristics are only applied to the nuclear power plants. From the optimization solution, we see that the nuclear plants are consistently operated at full capacity. This can be explained by its lowest levelized cost of electricity among the generation technologies. We have not considered the alternative to decarbonize traditional thermal plants with carbon capture. However, they might perform similarly to the nuclear plants in this case, acting as a base load when solar and wind capacities have reached their limits, while the electricity grid and storage systems handle the fluctuations.

Table 2
Solution time, objective value, and feasibility test results of different characteristic combinations.

Benchmark	Solution time		Objective value			
	IEEE	NL8	IEEE	NL8		
-ref	1.4 h	16.6 h	4.9×10^8 $	1.1×10^{10} €		
Model	Difference in solution time		Difference in objective value		Feasibility test	
	IEEE	NL8	IEEE	NL8	IEEE	NL8
-EB	−78.2%	−99.8%	−0.2%	−63.1%	No	No
-lossless	−99.7%	−88.3%	−0.9%	−29.3%	No	No
-free_ramp	−41.9%	−18.4%	−0.2%	+0%	Pass	Pass
-free_unit	−95.9%	−63.2%	−0.6%	+0%	Pass	Pass
-1Pconnect	−69.7%	−91.5%	+1.8%	−4.6%	Pass	No
-2Pconnect	−91.5%	−92.4%	+0.9%	+0.9%	Pass	Pass
-3Pconnect	−67.6%	−68.1%	+0.5%	+0.3%	Pass	Pass
-1Ptangent	−99.1%	−17.6%	−0.8%	−2.3%	No	No
-2Ptangent	−96.0%	−19.0%	−0.5%	−0.8%	No	No
-3Ptangent	−76.9%	−42.8%	−0.3%	−0.3%	No	No

Specifications of the characteristics can be found in Table 1.

4.2. Effects on the objective value, solution time and feasibility of the system capacity design

The optimal objective values reflect the impacts on the system capacity design. Table 2 shows that, for IEEE 118-Bus, all simplifications provide good approximations of the objective value. Nevertheless, having an accurate objective value does not guarantee the solution quality, as IEEE-EB and IEEE-lossless give negative results in the feasibility test. This means that even with a fixed transmission network, the dislocations and under-capacities of the generation and storage capacities caused by the network characteristics pose nontrivial challenges to the solution quality.

For NL-8-Node, Table 2 also confirms that the objective values of NL8-EB and NL8-lossless deviate the most from the reference. These designs turn out to be infeasible in the feasibility test. This implies that the solution for NL-8-Node, which optimizes the transmission network design alongside generation and storage, is more sensitive to the AC power transmission characteristics than the IEEE 118-Bus, whose transmission network is fixed. The difference in AC power transmission is evident from Fig. 9, where most of the power flows in IEEE-ref are below 20% of the line thermal capacities, while AC transmission flows in NL8-ref are mostly over 60%. This also explains the peculiarity observed in Table 2: the IEEE-1Pconnect produces a feasible system design, while the NL8-1Pconnect does not. As shown in Fig. 2, the 1Pconnect approximation overestimates AC transmission loss below 75% of the line capacity and underestimates them above that threshold. Combining with Fig. 9, in the IEEE-1Pconnect case, most per-unit AC power flows remain well below 75%, resulting in only a slight (1.8%) increase in the objective value. Whereas the NL8 has flows mostly above 75%, leading to a 4.6% undershoot of the objective value. This is caused by underinvestment in the capacities, ultimately leading to an infeasible system design.

Unexpectedly, for both systems, removing any of the generator flexibility characteristics does not lead to infeasibility or large discrepancies in the objective value. What we observe is that for these two systems, the on-off status of thermal generators does not change frequently, and their output levels are mostly within the ramp rate limits.

Regarding the solution time shown in Table 2, the two systems exhibit contrasting tendencies. Using EB or lossless approximations significantly lowers solution times by more than 78.2% on both systems. However, the reduction by EB is stronger in the NL-8-Node than IEEE 118-Bus. A plausible explanation is that IEEE 118-Bus does not have options to change the electricity grid. Including KVL is more computationally challenging for the co-optimization of transmission and generation in NL-8-Node. Additionally, the difference in the impact of ignoring losses can be attributed to the usage of the network. The limited choices of generator and storage capacity for each bus in the IEEE 118-Bus test system mean that demands are satisfied by electricity transmitted from other buses. In contrast, NL-8-Node supplies its demands more locally, which can be seen by comparing the capacities of energy transmission lines with those of conversion technologies.

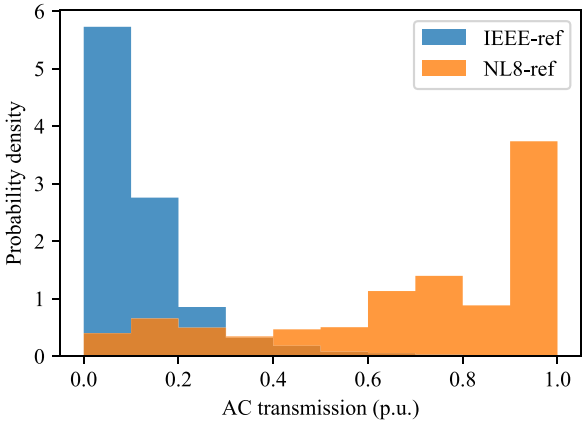

Fig. 9. Probability density of AC power flow in IEEE-ref and NL8-ref.

The contrasting impacts on the solution time of the two systems persist with the generator flexibility characteristics. The free_unit of NL-8-Node experiences a 63.2% reduction of computation time, while a 95.9% reduction is observed on IEEE-free_unit. This discrepancy is plausible because, in IEEE 118-Bus, the system is predominantly composed of thermal generators, whereas in NL-8-Node, only the nuclear plants are modeled with unit commitments.

In terms of the ramp rate limit, its removal reduces solution time more significantly in NL-8-Node than in IEEE 118-Bus test system. The reason is that in IEEE 118-Bus, the ramp rate limit constraints are not often binding, and the generators' power output varies mostly within the ramp rate limit. This is evident in Fig. 10, which displays the power output ramp rate normalized by the generators' limits. Even without imposing ramp rate limits, most fluctuations in power output do not reach limits. An implication is that other factors, like KVL and energy balances, more frequently dictate the generators' power output.

Summarizing the results above, we have provided evidence for the ESOM designers when, generally, considering the inclusion of system characteristics. This is because we find similarities between the two drastically different case studies. Especially regarding the inclusion of KVL and the AC transmission loss, we see from Table 2 that both systems become infeasible without them. This is due to the relaxation of the geographical requirement for the invested technology mix, which

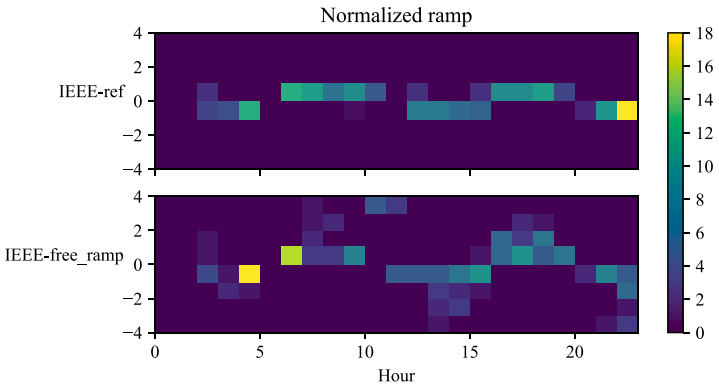

Fig. 10. Counts of generator ramp rate normalized by its ramp rate limit in IEEE-ref and IEEE-free_ramp.

is relatively obvious in NL-8-Node (Fig. 8) and with critical minutiae in IEEE 118-Bus (Fig. 6). Even for no-investment ESOMs, the relaxed network can enable infeasible generation scheduling, which, if adopted by a grid operator, would lead to economic losses and, to some extent, increase the risk to grid security. Therefore, despite the significant rise in complexity, reflected by the solution time, we strongly recommend including them when building ESOMs. On the other hand, the generator flexibility characteristics have smaller impacts on the solution quality; hence, the additional computational burden they introduce must be considered case-by-case.

4.3. AC transmission loss approximations

Including AC electricity transmission losses is decisive to the solution feasibility of both the IEEE 118-Bus and the NL-8-Node systems, and it brings significant computational costs. In this section, we further explore multiple simplifications. This is done by using the linear tangent or quadratic connect methods previously described in Section 2.3, with 1, 2 or 3 pieces to compare with the reference model, which uses 10 pieces.

The effects of these simplifications on the solution objective value and feasibility are shown in Table 2. For the IEEE 118-Bus, the tangent approximations up to 3 pieces result in infeasible solutions, despite the high accuracy in the objective values. Revisiting the loss approximations in Fig. 2, as the number of pieces increases to 3, tangents do not appear to be more inaccurate than the quadratic connect method, yet it brings us infeasible solutions. We hypothesize that the key lies in the "free region" encircled in red. When such a "free region" exists, the modeled system can always transport cost-free a certain amount of electricity from anywhere to anywhere in the system. This leads to an infeasible system capacity design in the feasibility test.

Linearizing the quadratic transmission losses by connecting points rather than drawing tangents also performs better for the NL-8-Node case study. All tangent approximations give infeasible solutions again. Also in the connect group, however, an infeasible solution occurs on NL8-1Pconnect, i.e., when only one line is used. This is likely due to the inaccuracy of 1Pconnect, especially with a large amount of power flows close to the maximum capacity, as in Fig. 9.

When it comes to the solution times, connect approximations outperform the tangents. One explanation is that having the slope from the origin, as visible in Fig. 2, gives one less vertex than the tangent, which later helps in the solution process of the linear optimization problem. Interestingly, we observe that the solution time decreases as the number of tangent lines increases. It can be explained by the reduction in the "free" flow region gradually strengthens the preference for local generation, which reduces the complexity of the power transmission decisions.

4.4. Limitations of this study

A limitation of this work is that the results are derived from two case studies, though they are contrastingly different from each other. There could be scenarios where the characteristics deemed less important in our study play more substantial roles. For example, in the energy system cases presented in [15] with a stronger focus on thermal generator unit commitment, the generator flexibility characteristics have higher impacts on the solution quality. However, our NL-8-Node case design aims to represent future decarbonized energy systems, characterized by high levels of renewable energy penetration and various storage technologies. The work in Helistö et al. [5] has demonstrated that a significant share of renewable energy, often offering options to curtail its output, can diminish the need for modeling the operational limits of thermal generators. Likewise, Poncelet et al. [59] suggest that when storage technologies provide flexibility in the system, detailed modeling of thermal generators becomes less important to the solution quality. Hence, it is not surprising that our research discovered similar trends.

When modeling the planning of the electricity transmission network in the NL-8-Node system, we ignore the N-1 security constraints, which are commonly applied in power system studies [60]. The N-1 security constraints, which impose requirements for the system to ensure reliable operation under a contingency affecting any system component, including generators, lines, and transformers [61], are not aligned with the level of abstraction in the NL-8-Node system. Modeling the system in detail down to the component level would introduce an excessive computational burden and could be prohibitive in large-scale studies.

5. Conclusion and recommendations

In this study, we systematically assessed the need to include electrical power transmission and generator flexibility characteristics in energy system optimization models and applied these modeling ideas to the IEEE 118-Bus test system and a self-sufficient zero-emission multi-energy system for the Netherlands. The literature lacks both the systematic evaluation of these characteristics and the comparison between electrical and multi-energy systems. As energy sectors become increasingly integrated, our study offers recommendations for the selection of the physical characteristics and approaches to model electricity transmission and associated losses in a multi-energy system.

We identify that for both systems, the modeling of network characteristics, i.e. the Kirchhoff's voltage law (KVL) and the electricity transmission losses, plays more crucial roles than generator flexibility characteristics. These include the ramp rate limits and unit commitment with minimum up and down times, together with generator startup and shutdown trajectories. Disregarding the network characteristics can bring large discrepancies in objective values and infeasible system designs; this was observed in both the IEEE 118-Bus system with 186 alternating current (AC) lines and the NL-8-Node system with only

7 possible AC connections. On the other hand, removing generator flexibility characteristics might not impact the objective values or the solution feasibility as much, depending on the technology capabilities and system requirements. Based on the results, we recommend (i) to include the modeling of the electrical circuit and the transmission losses, (ii) to decide upon the need for generator flexibility characteristics depending on the specific characteristics of the problem under evaluation (e.g., necessary in a technology-oriented analysis).

The optimal system design, especially the transmission network, if included in the optimization problem, is significantly influenced by the modeling of KVL. We observe that when considering KVL, the optimal solution avoids constructing closed loops in the transmission network. Otherwise, the system would have a more connected network, which might be less practical or operable in reality.

In the linear approximations of the AC transmission loss, we point out a potential pitfall. Linearizing the quadratic loss with tangents of up to 3 pieces can result in an infeasible system design, potentially due to the modeling error of creating a lossless region. Our results demonstrate that this is an issue in both systems, despite their drastically different power transmission intensities. Moreover, compared to connecting the points in the quadratic loss, tangent approximations lead to a higher solution time by a factor of 2–10. Utilizing more than one piece in the connect approximations gives both accurate and feasible solutions.

This work highlights the need for modeling the power network and associated transmission losses in multi-energy system design problems, while uncovering a pitfall in the linearization of the power transmission loss. The results provide guidance for problem designers to prioritize the physical characteristics and avoid unnecessary computational burdens. We encourage future research in this direction to explore the characteristics with finer granularity in temporal resolution (under 1 h) and multiple, more detailed models of physical characteristics. Such an investigation would contribute further to enhancing the solution quality of energy system capacity and operation planning.

CRediT authorship contribution statement

Zhi Gao: Writing – original draft, Visualization, Methodology, Investigation, Formal analysis, Data curation, Conceptualization. **Germán Morales-España:** Writing – review & editing, Validation, Supervision, Methodology, Funding acquisition, . **Madeleine Gibescu:** Writing – review & editing, Supervision, Investigation, Funding acquisition, . **Matteo Gazzani:** Writing – review & editing, Visualization, Validation, Supervision, Methodology, Investigation, Funding acquisition, Conceptualization.

Declaration of Generative AI and AI-assisted technologies in the writing process

During the preparation of this work, the author(s) used ChatGPT in order to proofread the manuscript. After using this tool/service, the author(s) reviewed and edited the content as needed and take(s) full responsibility for the content of the publication.

Declaration of competing interest

The authors declare that they have no known competing financial interests or personal relationships that could have appeared to influence the work reported in this paper.

Acknowledgments

This publication is part of the project NextGenOpt with project number ESI.2019.008, which is (partly) financed by the Dutch Research Council (NWO), and supported by eScience Center under project numberNLeSC C 21.0226.

Appendix A. Additional node input data in NL-8-node

Table A.1
Distance between each of two onshore nodes in NL-8-Node.

Node 1	Node 2	L (km)
N	M	160
	ME	110
M	ME	100
	S	90
	SE	100
ME	SE	100
S	SE	110

Table A.2
Economic parameters of the energy transport infrastructure. Parameters of HVAC are taken from [62], HVDC from [63] and [64], and hydrogen pipeline from [65].

Transport technology	Y (years)	$\tilde{C}^{I}$ (€/MW km)	FOM
HVAC	40	400	2%
HVDC with inverters	40	2000	0.35%
Hydrogen pipeline	40	267	3%

Table A.3
Electrical properties for overhead HVAC lines [39].

V (kV)	$\tilde{R}$ (Ω/km)	$\tilde{X}$ (Ω/km)	$\overline{F}$ (MVA)
380	0.03	0.246	1698

Table A.4
Land resources in NL-8-Node.

Node	Solar area (m^2)	Wind Area (m^2)
N	27,590,000	1,078,993
M	69,500,000	848,870
ME	45,510,000	1,039,203
S	6,580,000	2,778,724
SE	50,810,000	690,844
OS-N	N/A	1,413,333
OS-M	N/A	4,462,933
OS-S	N/A	400,667

Table A.5
Design wind speeds of wind turbines, adapted from [66].

$V^{\text{cut-in}}$ (m/s)	V^{rated} (m/s)	$V^{\text{cut-out}}$(m/s)
4	16	25

Table A.6
Parameters of the nuclear power plant units. Ramp-rate limits are assumed to be 0.3, similar to historically used values [67]. The rest are adapted from [68].

RU, RD	$\underline{P}$ (MW)	$\overline{P}$ (MW)
0.3	785	1570
TU (h)	TD (h)	SUD, SDD (h)
8	24	2

Table A.7
Economic parameters of all technology types considered in the NL 8-node case study. Parameters of the nuclear plant are taken from [69] and [67]. The rest are acquired from [54].

Technology	Nodes	Y	$\tilde{C}^{I}$ (€/kW)	FOM	C^{O} (€/MWh)	C^{SU} (€)
On-shore wind turbine	N, M, ME, S, SE	30	1020	1.2%	1.3	N/A
Off-shore wind turbine	OS-N, OS-M, OS-S	30	1641	2.3%	3.25	N/A
PV panel	N, M, ME, S, SE	40	845	1.22%	0	N/A
Alkaline electrolyzer	N, M, ME, S, SE	25	300	4%	0	N/A
Solid oxide fuel cell	N, M, ME, S, SE	20	850	5%	0	N/A
Nuclear plant	S	60	6000	1.4%	11.5	78,500
Li-ion battery	N, M, ME, S, SE	30	220	0.2%	1.7	N/A
Hydrogen tank	S	30	275	1.5%	0	N/A
Salt cavern	N	100	4	0	0	N/A

Data availability

Data is available from [14] [37], as also provided in the manuscript.

References

[1] International Energy Agency. Net zero by 2050. 2021, https://www.iea.org/reports/net-zero-by-2050.

[2] Intergovernmental Panel on Climate Change. Synthesis report. contribution of working groups i, ii and iii to the sixth assessment report of the intergovernmental panel on climate change. Clim Chang 2023;2023:35–115. http://dx.doi.org/10.59327/IPCC/AR6-9789291691647, https://www.ipcc.ch/report/ar6/syr/.

[3] Wuijts R, Akker J, Broek M. Effect of modelling choices in the unit commitment problem. Energy Syst 2023. http://dx.doi.org/10.1007/s12667-023-00564-5.

[4] Fattahi A, Sánchez Diéguez M, Sijm J, Morales España G, Faaij A. Measuring accuracy and computational capacity trade-offs in an hourly integrated energy system model. Adv Appl Energy 2021;1:100009. http://dx.doi.org/10.1016/j.adapen.2021.100009, https://www.sciencedirect.com/science/article/pii/S2666792421000020.

[5] Helistö N, Kiviluoma J, Morales-España G, O'Dwyer C. Impact of operational details and temporal representations on investment planning in energy systems dominated by wind and solar. Appl Energy 2021;290:116712. http://dx.doi.org/10.1016/j.apenergy.2021.116712, https://www.sciencedirect.com/science/article/pii/S0306261921002312.

[6] Guo F, van Ruijven BJ, Zakeri B, Zhang S, Chen X, Liu C, et al. Implications of intercontinental renewable electricity trade for energy systems and emissions. Nat Energy 2022;7:1144–56. http://dx.doi.org/10.1038/s41560-022-01136-0.

[7] Wogrin S, Tejada-Arango D, Delikaraoglou S, Botterud A. Assessing the impact of inertia and reactive power constraints in generation expansion planning. Appl Energy 2020;280:115925. http://dx.doi.org/10.1016/j.apenergy.2020.115925, https://www.sciencedirect.com/science/article/pii/S0306261920313842.

[8] Moradi-Sepahvand M, Amraee T. Integrated expansion planning of electric energy generation, transmission, and storage for handling high shares of wind and solar power generation. Appl Energy 2021;298:117137. http://dx.doi.org/10.1016/j.apenergy.2021.117137, https://www.sciencedirect.com/science/article/pii/S0306261921005778.

[9] Singh R, Bansal RC. Optimization of an autonomous hybrid renewable energy system using reformed electric system cascade analysis. IEEE Trans Ind Inform. 2019;15:399–409. http://dx.doi.org/10.1109/TII.2018.2867626.

[10] Zhang D, Zhu H, Zhang H, Goh HH, Liu H, Wu T. Multi-objective optimization for smart integrated energy system considering demand responses and dynamic prices. IEEE Trans Smart Grid 2022;13:1100–12. http://dx.doi.org/10.1109/TSG.2021.3128547.

[11] Ringkjøb H-K, Haugan PM, Solbrekke IM. A review of modelling tools for energy and electricity systems with large shares of variable renewables. Renew Sustain Energy Rev 2018;96:440–59. http://dx.doi.org/10.1016/j.rser.2018.08.002, https://www.sciencedirect.com/science/article/pii/S1364032118305690.

[12] Neumann F, Hagenmeyer V, Brown T. Assessments of linear power flow and transmission loss approximations in coordinated capacity expansion problems. Appl Energy 2022;314:118859. http://dx.doi.org/10.1016/j.apenergy.2022.118859, https://www.sciencedirect.com/science/article/pii/S0306261922002938.

[13] Alizadeh M, Parsa Moghaddam M, Amjady N, Siano P, Sheikh-El-Eslami M. Flexibility in future power systems with high renewable penetration: A review. Renew Sustain Energy Rev 2016;57:1186–93. http://dx.doi.org/10.1016/j.rser.2015.12.200, https://www.sciencedirect.com/science/article/pii/S136403211501583X.

[14] Tejada-Arango DA, Morales-España G, Wogrin S, Centeno E. Power-based generation expansion planning for flexibility requirements. IEEE Trans Power Syst 2020;35:2012–23. http://dx.doi.org/10.1109/TPWRS.2019.2940286.

[15] Wuijts R, van den Akker M, van den Broek M. Effect of modelling choices in the unit commitment problem. Energy Syst 2023. http://dx.doi.org/10.1007/s12667-023-00564-5.

[16] Shirizadeh B, Quirion P. Do multi-sector energy system optimization models need hourly temporal resolution? a case study with an investment and dispatch model applied to france. Appl Energy 2022;305:117951. http://dx.doi.org/10.1016/j.apenergy.2021.117951, https://www.sciencedirect.com/science/article/pii/S0306261921012617.

[17] Gabrielli P, Gazzani M, Martelli E, Mazzotti M. Optimal design of multi-energy systems with seasonal storage. Appl Energy 2018;219:408–24. http://dx.doi.org/10.1016/j.apenergy.2017.07.142, https://www.sciencedirect.com/science/article/pii/S0306261917310139.

[18] Kotzur L, Markewitz P, Robinius M, Stolten D. Time series aggregation for energy system design: Modeling seasonal storage. Appl Energy 2018;213:123–35. http://dx.doi.org/10.1016/j.apenergy.2018.01.023, https://www.sciencedirect.com/science/article/pii/S0306261918300242.

[19] Kiaee M, Cruden A, Chladek P, Infield D. Demonstration of the operation and performance of a pressurised alkaline electrolyser operating in the hydrogen fuelling station in Porsgrunn, Norway. Energy Convers Manage 2015;94:40–50. http://dx.doi.org/10.1016/j.enconman.2015.01.070, https://www.sciencedirect.com/science/article/pii/S0196890415000837.

[20] Stansberry JM, Brouwer J. Experimental dynamic dispatch of a 60 kw proton exchange membrane electrolyzer in power-to-gas application. Int J Hydrog Energy 2020;45:9305–16. http://dx.doi.org/10.1016/j.ijhydene.2020.01.228, https://www.sciencedirect.com/science/article/pii/S0360319920304237.

[21] Martinez Lopez V, Ziar H, Haverkort J, Zeman M, Isabella O. Dynamic operation of water electrolyzers: A review for applications in photovoltaic systems integration. Renew Sustain Energy Rev 2023;182:113407. http://dx.doi.org/10.1016/j.rser.2023.113407, https://www.sciencedirect.com/science/article/pii/S1364032123002642.

[22] Varela C, Mostafa M, Zondervan E. Modeling alkaline water electrolysis for power-to-x applications: A scheduling approach. Int J Hydrog Energy 2021;46:9303–13. http://dx.doi.org/10.1016/j.ijhydene.2020.12.111, https://www.sciencedirect.com/science/article/pii/S036031992034725X.

[23] Luo Y, Jiao K. Cold start of proton exchange membrane fuel cell. Prog Energy Combust Sci 2018;64:29–61. http://dx.doi.org/10.1016/j.pecs.2017.10.003, https://www.sciencedirect.com/science/article/pii/S0360128517300175.

[24] Nikiforow K, Pennanen J, Ihonen J, Uski S, Koski P. Power ramp rate capabilities of a 5kw proton exchange membrane fuel cell system with discrete ejector control. J Power Sources 2018;381:30–7. http://dx.doi.org/10.1016/j.jpowsour.2018.01.090, https://www.sciencedirect.com/science/article/pii/S0378775318300995.

[25] Teichgraeber H, Brandt AR. Time-series aggregation for the optimization of energy systems: Goals, challenges, approaches, and opportunities. Renew Sustain Energy Rev 2022;157:111984. http://dx.doi.org/10.1016/j.rser.2021.111984, https://www.sciencedirect.com/science/article/pii/S1364032121012478.

[26] Kotzur L, Markewitz P, Robinius M, Stolten D. Impact of different time series aggregation methods on optimal energy system design. Renew Energy 2018;117:474–87. http://dx.doi.org/10.1016/j.renene.2017.10.017, https://www.sciencedirect.com/science/article/pii/S0960148117309783.

[27] Weimann L, Gazzani M. A novel time discretization method for solving complex multi-energy system design and operation problems with high penetration of renewable energy. Comput Chem Eng 2022;163:107816. http://dx.doi.org/10.1016/j.compchemeng.2022.107816, https://www.sciencedirect.com/science/article/pii/S0098135422001545.

[28] Hoffmann M, Kotzur L, Stolten D, Robinius M. A review on time series aggregation methods for energy system models. Energies 2020;13. http://dx.doi.org/10.3390/en13030641, https://www.mdpi.com/1996-1073/13/3/641.

[29] Priesmann J, Nolting L, Praktiknjo A. Are complex energy system models more accurate? an intra-model comparison of power system optimization models. Appl Energy 2019;255:113783. http://dx.doi.org/10.1016/j.apenergy.2019.113783, https://www.sciencedirect.com/science/article/pii/S0306261919314709.

[30] Stott B, Jardim JL, Alsac O. Dc power flow revisited. IEEE Trans Power Syst 2009;24:1290–300, https://api.semanticscholar.org/CorpusID:42572597.

[31] Molzahn DK, Hiskens IA. A survey of relaxations and approximations of the power flow equations. 2019.
[32] Morales-España G, Tejada-Arango DA. Modeling the hidden flexibility of clustered unit commitment. IEEE Trans Power Syst 2019;34:3294–6. http://dx.doi.org/10.1109/TPWRS.2019.2908051.
[33] Meus J, Poncelet K, Delarue E. Applicability of a clustered unit commitment model in power system modeling. IEEE Trans Power Syst 2018;33:2195–204. http://dx.doi.org/10.1109/TPWRS.2017.2736441.
[34] Gentile C, Morales-España G, Ramos A. A tight mip formulation of the unit commitment problem with start-up and shut-down constraints. EURO J Comput Optim 2017;5:177–201. http://dx.doi.org/10.1007/s13675-016-0066-y, https://www.sciencedirect.com/science/article/pii/S2192440621000782.
[35] Morales-España G, Latorre J, Ramos A. Tight and compact milp formulation of start-up and shut-down ramping in unit commitment. IEEE Trans Power Syst 2012;28:1288–96. http://dx.doi.org/10.1109/TPWRS.2012.2222938.
[36] Illinois Center for a Smarter Electric Grid. IEEE 118bus system. 2023, https://icseg.iti.illinois.edu/ieee-118-bus-system/.
[37] Gao Z. Case study for comparison of system characteristics. 2024, https://github.com/gzclarence/EnergyPowerCharacteristics/tree/main.
[38] Weimann L, Gabrielli P, Boldrini A, Kramer GJ, Gazzani M. Optimal hydrogen production in a wind-dominated zero-emission energy system. Adv Appl Energy 2021;3:100032. http://dx.doi.org/10.1016/j.adapen.2021.100032, https://www.sciencedirect.com/science/article/pii/S2666792421000251.
[39] Oeding D, Oswald B. Elektrische kraftwerke und netze. Springer Berlin Heidelberg; 2016, https://link.springer.com/book/10.1007/978-3-662-52703-0.
[40] nationalgrid. High voltage direct current electricity – technical information. 2024, https://www.nationalgrid.com/sites/default/files/documents/13784-High%20Voltage%20Direct%20Current%20Electricity%20%E2%80%93%20technical%20information.pdf.
[41] Tsiklios C, Hermesmann M, Müller T. Hydrogen transport in large-scale transmission pipeline networks: Thermodynamic and environmental assessment of repurposed and new pipeline configurations. Appl Energy 2022;327:120097. http://dx.doi.org/10.1016/j.apenergy.2022.120097, https://www.sciencedirect.com/science/article/pii/S030626192201354X.
[42] Guidehouse. European hydrogen backbone. 2022, https://gasforclimate2050.eu/wp-content/uploads/2022/04/EHB-A-European-hydrogen-infrastructure-vision-covering-28-countries.pdf.
[43] Centraal Bureau voor de Statistiek. How do we use our land?. 2022, https://longreads.cbs.nl/the-netherlands-in-numbers-2021/how-do-we-use-our-land/.
[44] Centraal Bureau voor de Statistiek. How many wind turbines in the netherlands?. 2022, https://longreads.cbs.nl/the-netherlands-in-numbers-2022/how-many-wind-turbines-in-the-netherlands/.
[45] Noordzeeloket. Offshore wind energy road map. 2023, https://www.noordzeeloket.nl/en/functions-and-use/offshore-wind-energy/.
[46] National Renewable Energy Laboratory, USDepartment of Energy. Best research-cell efficiency chart. 2023, https://www.nrel.gov/pv/cell-efficiency.html.
[47] Frantál B, Frolova M, Liñán-Chacón J. Conceptualizing the patterns of land use conflicts in wind energy development: Towards a typology and implications for practice. Energy Res Soc Sci 2023;95:102907. http://dx.doi.org/10.1016/j.erss.2022.102907, https://www.sciencedirect.com/science/article/pii/S2214629622004108.
[48] Jerez S, Thais F, Tobin I, Wild M, Colette A, Yiou P, et al. The climix model: A tool to create and evaluate spatially-resolved scenarios of photovoltaic and wind power development. Renew Sustain Energy Rev 2015;42:1–15. http://dx.doi.org/10.1016/j.rser.2014.09.041, https://www.sciencedirect.com/science/article/pii/S1364032114008144.
[49] Koninklijk Nederlands Meteorologisch Instituut. Meteo data - actual synoptic observations knmi the netherlands per 10 min. 2023, https://dataplatform.knmi.nl/dataset/actuele10mindataknmistations-2.
[50] US Department of Energy. Fuel cells fact sheet. 2015, https://www.energy.gov/eere/fuelcells/articles/fuel-cells-fact-sheet.
[51] Shiva Kumar S, Himabindu V. Hydrogen production by pem water electrolysis – a review. Mater Sci Energy Technol 2019;2:442–54. http://dx.doi.org/10.1016/j.mset.2019.03.002, https://www.sciencedirect.com/science/article/pii/S2589299119300035.
[52] World Nuclear News. Borssele earmarked for two new reactors. 2022, https://world-nuclear-news.org/Articles/Borssele-earmarked-for-two-new-reactors.
[53] Reuters. Netherlands talking to three suppliers to build new nuclear power plants. 2023, https://www.reuters.com/business/energy/netherlands-talking-three-suppliers-build-new-nuclear-power-plants-2023-06-29/.
[54] Danish Energy Agency. Technology data. 2023, https://ens.dk/en/our-services/projections-and-models/technology-data.
[55] Luo X, Wang J, Dooner M, Clarke J. Overview of current development in electrical energy storage technologies and the application potential in power system operation. Appl Energy 2015;137:511–36. http://dx.doi.org/10.1016/j.apenergy.2014.09.081, https://www.sciencedirect.com/science/article/pii/S0306261914010290.
[56] Elberry AM, Thakur J, Santasalo-Aarnio A, Larmi M. Large-scale compressed hydrogen storage as part of renewable electricity storage systems. Int J Hydrog Energy 2021;46:15671–90. http://dx.doi.org/10.1016/j.ijhydene.2021.02.080, https://www.sciencedirect.com/science/article/pii/S0360319921005838.
[57] Pyomo. Pyomo. 2025, http://www.pyomo.org/.
[58] Gurobi. Gurobi opimization. 2025, https://www.gurobi.com/.
[59] Poncelet K, Delarue E, D'haeseleer W. Unit commitment constraints in long-term planning models: Relevance, pitfalls and the role of assumptions on flexibility. Appl Energy 2020;258:113843. http://dx.doi.org/10.1016/j.apenergy.2019.113843, https://www.sciencedirect.com/science/article/pii/S0306261919315302.
[60] He C, Wu L, Liu T, Bie Z. Robust co-optimization planning of interdependent electricity and natural gas systems with a joint n-1 and probabilistic reliability criterion. IEEE Trans Power Syst 2018;33:2140–54. http://dx.doi.org/10.1109/TPWRS.2017.2727859.
[61] IEA. Strengthening power system security in kyrgyzstan: A roadmap. 2022, https://www.iea.org/reports/strengthening-power-system-security-in-kyrgyzstan-a-roadmap.
[62] Hagspiel S, Jägemann C, Lindenberger D, Brown T, Cherevatskiy S, Tröster E. Cost-optimal power system extension under flow-based market coupling. Energy 2014;66:654–66. http://dx.doi.org/10.1016/j.energy.2014.01.025, https://www.sciencedirect.com/science/article/pii/S0360544214000322.
[63] Härtel P, Vrana TK, Hennig T, von Bonin M, Wiggelinkhuizen EJ, Nieuwenhout FD. Review of investment model cost parameters for vsc hvdc transmission infrastructure. Electr Power Syst Res 2017;151:419–31. http://dx.doi.org/10.1016/j.epsr.2017.06.008, https://www.sciencedirect.com/science/article/pii/S0378779617302572.
[64] Purvins A, Sereno L, Ardelean M, Covrig C-F, Efthimiadis T, Minnebo P. Submarine power cable between Europe and North America: A techno-economic analysis. J Clean Prod 2018;186:131–45. http://dx.doi.org/10.1016/j.jclepro.2018.03.095, https://www.sciencedirect.com/science/article/pii/S0959652618307522.
[65] Welder L, Ryberg D, Kotzur L, Grube T, Robinius M, Stolten D. Spatio-temporal optimization of a future energy system for power-to-hydrogen applications in germany. Energy 2018;158:1130–49. http://dx.doi.org/10.1016/j.energy.2018.05.059, https://www.sciencedirect.com/science/article/pii/S036054421830879X.
[66] wind-turbine-models. Windturbines database. 2023, https://en.wind-turbine-models.com/turbines.
[67] Lynch A, Perez Y, Gabriel S, Mathonniere G. Nuclear fleet flexibility: Modeling and impacts on power systems with renewable energy. Appl Energy 2022;314:118903. http://dx.doi.org/10.1016/j.apenergy.2022.118903, https://www.sciencedirect.com/science/article/pii/S0306261922003282.
[68] Jenkins J, Zhou Z, Ponciroli R, Vilim R, Ganda F, de Sisternes F, et al. The benefits of nuclear flexibility in power system operations with renewable energy. Appl Energy 2018;222:872–84. http://dx.doi.org/10.1016/j.apenergy.2018.03.002, https://www.sciencedirect.com/science/article/pii/S0306261918303180.
[69] Gamboa Palacios S, Jansen J. Nuclear energy economics: An update to fact finding nuclear energy. 2018, https://repository.tno.nl/.